Geological Society of America Bulletin

The Kumaun and Garwhal Lesser Himalaya, India: Part 2. Thermal and deformation histories

Julien Célérier, T. Mark Harrison, Olivier Beyssac, Frédéric Herman, William J. Dunlap and A. Alexander G. Webb

Email alerting services	click www.gsapubs.org/cgi/alerts to receive free e-mail alerts when new articles cite this article
Subscribe	click www.gsapubs.org/subscriptions/ to subscribe to Geological Society of America Bulletin
Permission request	click http://www.geosociety.org/pubs/copyrt.htm#gsa to contact GSA

Notes

THE
GEOLOGICAL
SOCIETY
OF AMERICA

The Kumaun and Garwhal Lesser Himalaya, India:
Part 2. Thermal and deformation histories

Julien Célérier[1][†], T. Mark Harrison[1,2], Olivier Beyssac[3,4], Frédéric Herman[4,5], William J. Dunlap[1], and
A. Alexander G. Webb[2]

[1]*Research School of Earth Sciences, Australian National University, Canberra, ACT 0200, Australia*
[2]*Department of Earth and Space Sciences and Institute of Geophysics and Planetary Physics, University of California, Los Angeles, California 90095-1567, USA*
[3]*Laboratoire de Géologie, Ecole Normale Supérieure, CNRS-UMR 8538, 24 rue Lhomond, F-75005, Paris, France*
[4]*Tectonics Observatory, California Institute of Technology Pasadena, California 91125, USA*
[5]*Geological Institut, Earth Surface Dynamics Group, Department of Earth Sciences, ETH-Zürich, Haldenbachstrasse 44, CH-8092 Zürich, Switzerland*

ABSTRACT

An integrated petrologic, thermochronologic, and numerical modeling study constrains the thermal evolution of the Lesser Himalayan Sequence in the Kumaun and Garwhal regions of India. South of the Tons thrust, peak metamorphic temperatures do not exceed 330 °C. On the northern side, a transition toward higher temperatures adjacent to the Main Central thrust hanging wall is documented. In the immediate footwall of the Main Central thrust, peak temperatures average ~550 °C. An inverted thermal field gradient of ~30 °C/km beneath the Vaikrita thrust is calculated. An inverted thermal field gradient of ~20 °C/km is also documented beneath a klippe of the Main Central thrust hanging wall ~25 km south of the Vaikrita thrust, and a peak footwall temperature of 530 °C is recorded close to the shear zone at the base of the klippe. The mechanism for thermal metamorphism in the Lesser Himalayan Sequence is interpreted to be conduction of heat from the Main Central thrust fault and/or hanging wall to the footwall. A localized thermal field gradient is also associated with the Tons thrust. The $^{40}Ar/^{39}Ar$ thermochronology reveals that the exposed rock in the Kumaun and Garwhal Lesser Himalaya underwent cooling below the closure temperature (T_c) for white mica at different times in the late Tertiary. The proximal footwall of the Munsiari thrust experienced cooling below the white mica T_c at ca. 8.5 Ma. South of the Munsiari thrust, in the proximal footwalls of the Chaukori and Askot klippen, muscovites ages are ca. 11.5 Ma, ~3 Ma older than samples to the north. The age differences in samples from northern and southern exposures are interpreted to document cooling related to thermal relaxation following passage of the Main Central thrust hanging wall atop the Lesser Himalayan Sequence. Results of thermal modeling achieve good fits to the data when scenarios involve an early Miocene phase of overthrusting of a hot hanging wall over a downgoing footwall, followed by the initiation of a duplex within Lesser Himalayan Sequence rocks.

INTRODUCTION

Classical methods of investigating orogenic histories have focused largely on the sedimentary products of uplift and erosion (e.g., Dickinson, 1971) rather than on residual bedrock exposures. These approaches have more recently been supplemented by the recognition that bedrock outcrops preserve isotopic and petrological thermal history records of the deformation and exhumation processes that shaped their evolution in the mountain belt (Ernst, 1971; England and Thompson, 1984; Copeland et al., 1987; Braun, 2003). These developments have largely been pioneered in context of the Alpine-Himalayan belt, with particular emphasis on the India-Asian collision zone. However, coverage of thermochronologic investigations within the Himalaya is very uneven. The vast majority have been undertaken within the Greater Himalayan Crystalline Complex, a narrow belt of amphibolite-grade schists and gneisses that typically make up no more than a quarter of the Himalayan mountain belt. Owing to difficulties quantifying the petro-genesis of rocks at low metamorphic grade, our understanding of the rest of the chain is poor. This is especially true of the rocks that lie structurally below the broad ductile shear zone known as the Main Central thrust—the Lesser Himalayan Sequence (Fig. 1). The few studies to have quantified the thermal evolution of these rocks (south of the lower bounding fault of the Main Central thrust shear zone [Munsiari thrust]) have tended to focus on Nepal (Beyssac et al., 2004). In this study, we use an integrated petrologic, thermometric, and thermochronologic approach to quantify the thermal evolution of the Lesser Himalayan Sequence in the Kumaun and Garwhal regions of northwestern India. We then use these results to evaluate a range of tectonic scenarios using forward thermo-kinematic models.

Review of Structural Framework

In this study, we adopt the structural framework of LeFort (1996), who divided the Himalayan orogen into four major tectonometamorphic units: (1) the Siwalik Group, consisting of Neogene to Quaternary fluvial sediments of the Himalayan foreland basin (Auden, 1935); (2) the Proterozoic to Paleozoic Lesser Himalayan Sequence (LHS); (3) the Proterozoic to Ordovician Greater Himalayan Complex (GHC); and (4) the Proterozoic to Eocene Tethyan Himalayan Sequence (THS). Each of these units is delimited by a series of north-dipping fault systems. From south to north, these are the thrust-sense Main Frontal thrust (MFT), the thrust-sense Main Boundary thrust (MBT), the thrust-sense Main Central thrust (MCT), and the normal-sense South Tibetan detachment (STD). The Lesser

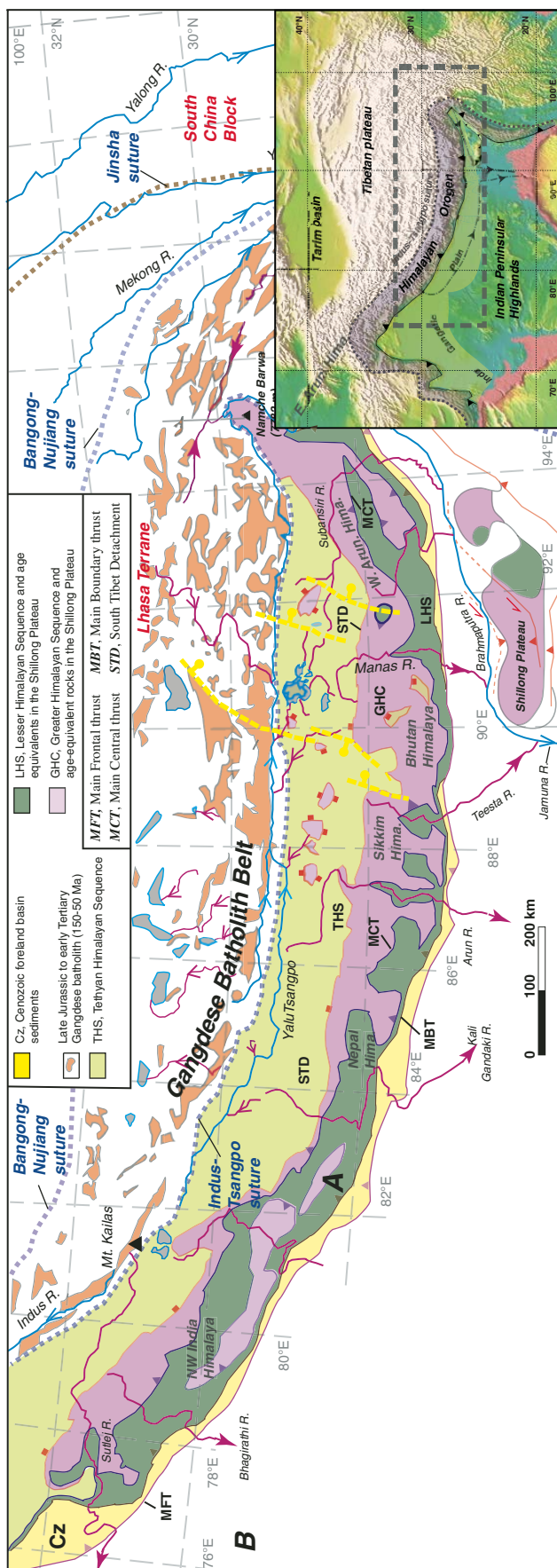[†]E-mail: juliencelerier@groundfloorgraphics.com

Figure 1. Simplified geological map of the Himalaya.

Himalayan Sequence has been further divided into a southern Neoproterozoic–Cambrian Outer sedimentary zone and a northern Meso- to Neoproterozoic Inner sedimentary zone separated by the south-dipping Tons thrust (Ahmad et al., 2000; Richards et al., 2005; Valdiya, 1980). The internal structural geology of the Lesser Himalayan Sequence is largely governed by the Ramgarh and Berinag thrusts (Fig. 2; Célérier et al., 2009). Defining the top of the Lesser Himalayan Sequence in the Uttaranchal region, the Main Central thrust has been further subdivided into upper and lower zones, the bounding faults of which are termed the Vaikrita and Munsiari thrusts, respectively (Valdiya, 1980). These two structures are equivalent to the Main Central thrust I and Main Central thrust II (Hashimoto et al., 1973) of Nepal. The reader is referred to the companion paper (Célérier et al., 2009) for a detailed description of the structural geology and stratigraphy of Uttaranchal. Table 1 provides a summary of the structural and stratigraphic terms referred to in the text.

Previous Studies of the Thermal Structure of the Lesser Himalaya

Metamorphic conditions in the Himalaya have largely been documented within the Greater Himalayan Complex, which record peak temperatures from ~550 °C to 750 °C along with an accompanying decrease in pressure upsection from 7–8 kbar to 3–4 kbar between the Main Central thrust and South Tibetan detachment (see reviews in Catlos et al., 2001; Harrison et al., 1999). Equally, much work has focused on understanding the thermal history of units within the Main Central thrust zone, i.e., between the Munsiari (MCT I) and Vaikrita thrusts (MCT II) (Catlos et al., 2001, 2007; Kohn et al., 2001, Vannay and Grasemann, 1998; Vannay et al., 2004). These studies have used various thermobarometric techniques based on cation partitioning (e.g., Ferry and Spear, 1978) to quantify pressure-temperature (*P-T*) conditions of metamorphism in the Main Central thrust zone of 520–650 °C and 6–10 kbar. However, south of the Munsiari thrust (structurally below the Main Central thrust ductile shear zone, within units of the Lesser Himalayan Sequence), where appropriate mineral assemblages for the application of thermobarometric techniques are lacking, metamorphic conditions have only been described qualitatively in terms of mineral isograds (Pêcher, 1989; Paudel and Arita, 2000). Recently, however, peak metamorphic temperatures in proximity to the Munsiari thrust and steep (20–50 °C/km) inverted thermal field gradients south of the Munsiari thrust have been documented in western and central
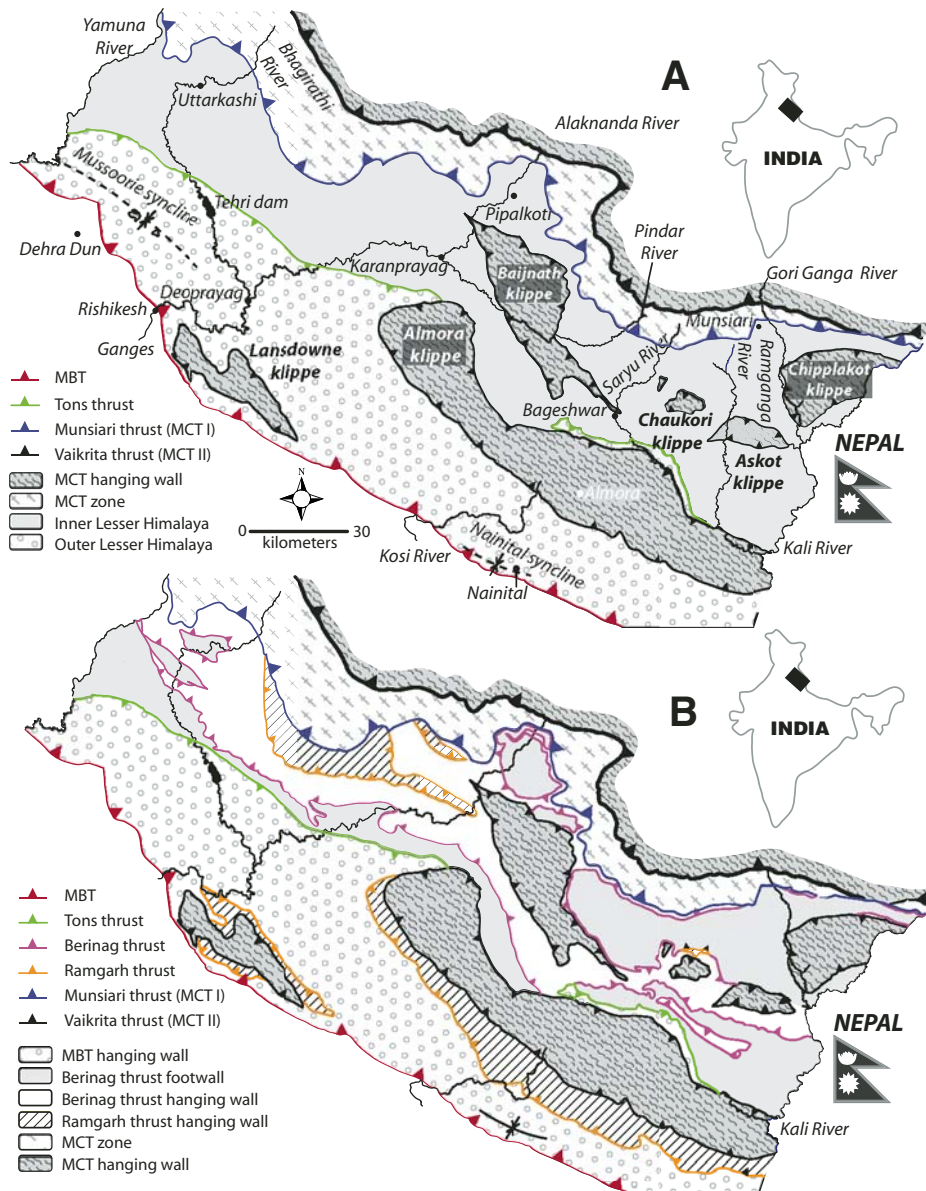
Figure 2. Structural architecture of the Kumaun and Garwhal Himalaya. (A) The first-order structure of the region showing a two-tiered stratigraphic sequence juxtaposed along the south-dipping Tons thrust. These metasediments are overlain by several klippen of the Main Central thrust hanging wall. Also shown are the major drainages and towns in the region. (B) Structure of the region as proposed by Valdiya (1980): a series of stacked thrust sheets.

Nepal using a method based on the structural state of carbonaceous material (Beyssac et al., 2004; Bollinger et al., 2004, 2006). These studies are of note because they were the first studies to quantitatively describe the conditions of metamorphism, and accompanying inverted thermal field gradients, in the Lesser Himalayan Sequence south of the Munsiari thrust. In this study, when referring to inverted thermal field gradients, we refer specifically to paleo-inverted thermal field gradients where peak

metamorphic temperatures decrease with distance structurally below the Main Central thrust.

The $^{40}Ar/^{39}Ar$ thermochronology method has been often applied to Himalayan samples to constrain cooling and denudation histories, with particular focus on the Greater Himalayan Complex and rocks adjacent to the Main Central thrust. In central Nepal, biotite $^{40}Ar/^{39}Ar$ ages (Copeland et al., 1991; Edwards, 1995) decrease from ca. 16 Ma in the upper Greater Himalayan Complex to as young as 2–3 Ma

within the Main Central thrust zone. Below the Munsiari thrust (MCT I), biotite ages increase rapidly to pre-Tertiary ages as old as 900 Ma (Copeland et al., 1991). Samples within the Main Central thrust zone yield scattered ages, and older samples generally exhibit age spectra suggestive of excess radiogenic $^{40}Ar^*$. Within the Kathmandu nappe (an eroded remnant of the Main Central thrust sheet preserved as a klippe in central Nepal), Arita et al. (1997) found a range of $^{40}Ar/^{39}Ar$ ages between 14 and 44 Ma for muscovites separated from granites and metasedimentary rocks. In eastern (Hubbard and Harrison, 1989) and western (Bollinger et al., 2004; Robinson et al., 2006) Nepal, similar $^{40}Ar/^{39}Ar$ age patterns have been documented. We are unaware of any $^{40}Ar/^{39}Ar$ data for the Lesser Himalayan Sequence sensu stricto in this area, i.e., south of the Munsiari thrust and structurally below the various klippen overlying the Lesser Himalayan Sequence.

THERMOMETRY AND THERMOCHRONOLOGY

We have characterized the thermal structure of the Lesser Himalayan Sequence by considering peak temperatures attained in metasedimentary rocks using Raman spectroscopy of carbonaceous material (RSCM) and thermochronological analysis of white micas. Before describing these results, we first note the presence of lineation-forming white mica, chlorite, and kyanite. White mica and chlorite become abundant in all Lesser Himalayan Sequence lithologies with proximity to the Munsiari thrust, as well as beneath the klippen to the north of the Tons thrust. Along the Alaknanda River (Fig. 3), kyanite is abundant in quartzites of the Berinag thrust's hanging wall, occurring within the quartzite matrix as well as on the margins of 5–30-cm-wide quartz veins cutting the northwest-dipping quartzites. Kyanite occurs as slightly elongate needles (<5 mm) parallel to the regional northwest-dipping foliation (shown in Fig. 3 partially replaced by lineation-forming muscovite). To the east, in the town of Munsiari, kyanite was observed within the matrices of quartzites in the proximal footwall of the Munsiari thrust (Célérier, 2007). Again, lineation-forming muscovite appears to have partially replaced the kyanite.

Raman Spectroscopy of Carbonaceous Material

Beyssac et al. (2002) calibrated a technique for the quantification of peak metamorphic temperatures without the limiting need in classical thermobarometric studies for specific mineral assemblages. The technique, Raman

TABLE 1. SUMMARY OF STRUCTURES AND
STRATIGRAPHIC INTERVALS COMMONLY REFERRED TO IN THE TEXT

Structure/Unit	Definition
Lesser Himalayan Sequence (LHS)	Proterozoic–Paleozoic low- to high-grade metasedimentary rocks including the *Inner* (northerly) and *Outer* (southerly) LHS.
Greater Himalayan Complex (GHC)	Proterozoic–Ordovician high-grade metasedimentary and meta-igneous rocks. Equivalent to Greater Himalayan Crystalline Series or Tibetan slab; sometimes subdivided into Formations I–III (structurally lowest to highest; Le Fort, 1975).
Main Himalayan thrust (MHT)	Master décollement beneath Himalayan wedge (Zhao et al., 1993; Hauck et al., 1998; Schulte-Pelkum et al., 2005), into which all thrusts are thought to sole.
Main Boundary thrust (MBT)	Thrust separating Proterozoic–Paleozoic rocks of the LHS from Tertiary foreland basin deposits of the Siwaliks.
Main Central thrust (MCT)	Collective term used to describe the broad fault zone separating the LHS and GHC.
MCT zone	Ductile shear zone bounded at its base by the Munsiari thrust and at its top by the Vaikrita thrust. It is within the MCT zone that much of the slip along the MCT has been accommodated.
Munsiari thrust	Thrust at the base of the MCT zone shown to have been active in the late Miocene–Pliocene by Harrison et al. (1997) and Catlos et al. (2004). Equivalent to the MCT I of Nepal (Hashimoto et al., 1973).
Vaikrita thrust	Thrust at the top of the MCT zone shown to have been active in the early Miocene (LeFort, 1975). Equivalent to the MCT II of Nepal (Hashimoto et al., 1973).
Berinag thrust	The Berinag thrust carries basal units of the *Inner* Lesser Himalaya over younger strata of the *Inner* Lesser Himalaya—typically Deoban Formation dolomites.
Ramgarh thrust	The Ramgarh thrust carries basal units of the *Outer* Lesser Himalaya over younger strata of the *Outer* Lesser Himalaya—typically Nagthat quartzites.
Tons thrust	Roughly halfway between the MBT and the Munsiari thrust, the Tons thrust (Valdiya, 1980) demarcates the boundary between the *Inner* and *Outer* Lesser Himalayan sequences of Ahmad et al. (2000).

Figure 3. Kyanite development in Berinag quartzites of the Lesser Himalayan Sequence along the Alaknanda River (GPS position: 30°31′05.1N, 79°29′48.8E). Kyanite within the recrystallized quartzite matrix is replaced by muscovite. Ky—kyanite, Qtz—quartz, Mu—muscovite.

spectroscopy of carbonaceous material (RSCM), is based upon the observation that sedimentary carbonaceous material is progressively transformed to graphite with increasing metamorphism. Beyssac et al. (2002) found a linear relationship between temperature and structural state quantified by Raman microspectroscopy in the range 330–640 °C, ranging from disordered carbonaceous material in low-metamorphic-grade samples to crystalline graphite in high-metamorphic-grade rocks (see GSA Data Repository for analytical details[1]).

Although the Kumaun and Garwhal Lesser Himalayan Sequence, south of the Munsiari thrust, are largely devoid of mineral assemblages suitable for conventional thermobarometry, graphitic schists are widespread. In total, 60 samples were analyzed from across Uttaranchal following the procedures detailed in Beyssac et al. (2002, 2003). Samples were analyzed using a Renishaw RM1000 at the California Institute of Technology and Renishaw Invia at the Ecole Normale Supérieure, Paris (analytical methods are described in GSA Data Repository [see footnote 1]).

The results of the RSCM thermometric study (Fig. 4) show three clusters of data from the Kumaun and Garwhal Lesser Himalaya samples. Sample coverage is densest in the east where graphitic schists are abundant. Another

cluster of data is centered in proximity to the Munsiari thrust along the Alaknanda River, where a window through the Berinag thrust hanging wall has exposed underlying dolomites and black schists of the Deoban and Mandhali Formations (Valdiya, 1980). In the west, exposure in the *Inner* Lesser Himalayan Sequence is dominated by Berinag quartzite, and so only sparse carbonaceous materials were available for sampling; to the south, several samples were analyzed from the Mussoorie syncline (Fig. 4).

In the east, relatively dense sampling of the Lesser Himalayan Sequence, north of the Tons thrust and between the Saryu and Kali Rivers, revealed a range of peak metamorphic temperatures between 340 °C and 580 °C (Fig. 4). Adjacent to the Munsiari thrust, peak metamorphic temperatures between 571 °C and 540 °C are recorded. Moving south along the Saryu River, a decrease of ~130 °C (549 °C to 416 °C) is recorded in the Lesser Himalayan Sequence over a map distance of 5.85 km. Further east, between the town of Munsiari and the northwest corner of the Chipplakot klippe, a cluster of samples was collected along the Gori Ganga River (Fig. 4). In this area, samples in the immediate proximity of the Munsiari thrust record peak temperatures of ~550 °C. Moving south again, temperature is essentially isothermal over a map distance of 11.30 km but increases to 580 °C within a distance of 1.30 km beneath the base of the Chipplakot klippe. Between these two transects, a southerly traverse from the town of Tejam toward the Askot klippe (along the Ram Ganga River) reveals an apparent inverted thermal field gradient to the south, away from
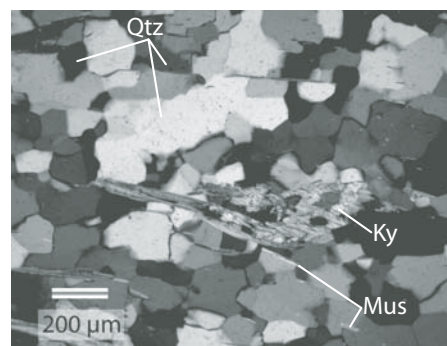
the Munsiari thrust but toward the sole thrust of the klippe (Fig. 4). Graphitic schists near Tejam (10.10 km map distance south of the Munsiari thrust) yielded peak metamorphic temperatures of ~370 °C, which provides a lower bound on the conditions of thermal metamorphism in this region of the *Inner* Lesser Himalayan Sequence. Between Tejam and the base of the Askot klippe, five samples record an increase in temperature of ~160 °C (373 °C to 531 °C) over 11.40 km map distance, defining an inverted thermal field gradient beneath the klippe. Approximately 25 km south of the Askot klippe (around the town of Pithoragarh), five data points include a maximum of ~395 °C decreasing to ~345 °C further south (Fig. 4).

The second cluster of samples is from along the upper reaches of the Alaknanda River, where a window through the Berinag thrust hanging wall exposes graphitic schists between the towns of Helang and Chamoli (Fig. 4). Within the window, peak metamorphic temperatures are essentially isothermal at ~510 °C. South of Chamoli, the northwest corner of the Baijnath klippe is exposed along the Alaknanda River. Analysis of graphitic schists within the Main Central thrust upper plate at this location yielded peak temperatures of ~575 °C. Further downstream, two exposures between Chamoli and the Tons thrust provided suitable material for RSCM, and both indicated temperatures of ~370 °C. Two samples of retrogressed, graphitic, schistose gneiss from within the Almora klippe yielded temperatures of 346 °C and 367 °C.

In the western sector, exposure of the *Inner* Lesser Himalayan Sequence is dominated by the hanging wall of the Berinag thrust sheet (Fig. 4), which does not contain suitable

[1]GSA Data Repository item 2009074, data tables presenting results of the Raman Spectroscopy of Carbonaceous Material and ⁴⁰Ar/³⁹Ar dating and details of the analytical methods used to generate Geochemical data, is available at http://www.geosociety.org/pubs/ft2008.htm or by request to editing@geosociety.org.
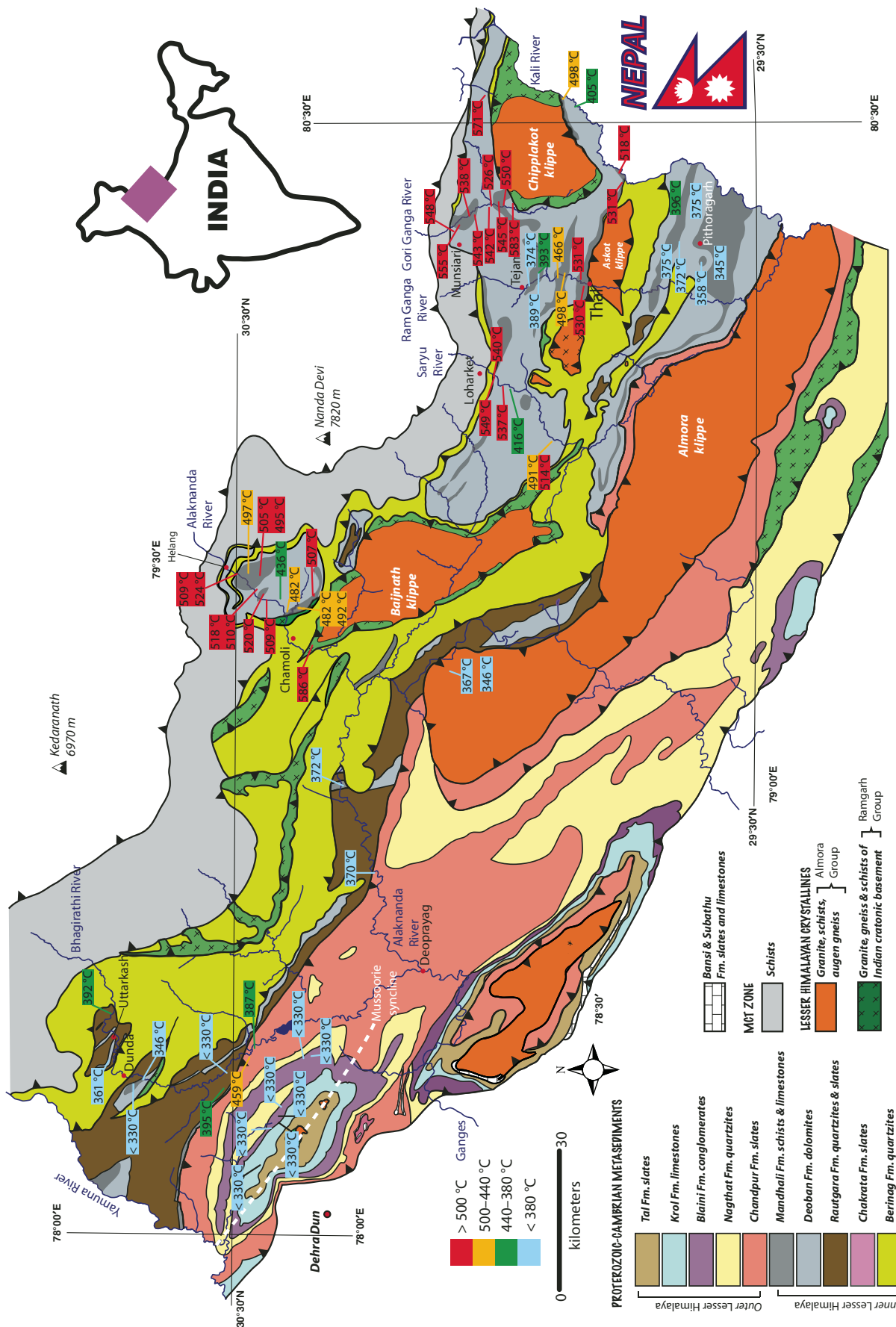
Figure 4. Geological map of the Kumaun and Garwhal Lesser Himalaya overlain with results of the Raman spectroscopy of carbonaceous material (RSCM) thermometric study.

lithologies for application of RSCM. However, two small windows along the Bhagirathi River (near the towns of Uttarkashi and Dunda) expose graphitic schists in the footwall of the Berinag thrust. In the more northerly window, two samples yielded temperatures of 360 °C and 390 °C (Fig. 4). Three samples from the southerly window were of low metamorphic grade; one sample yielded a temperature of 346 °C, and the other two samples were below the current calibration range of RSCM (i.e., <330 °C). In the *Outer* Lesser Himalayan Sequence, a suite of seven samples was taken across the axis of the Mussoorie syncline, and all yielded RSCM temperatures <330 °C. Between the *Inner* and *Outer* Lesser Himalayan Sequence, rocks in the vicinity of the Tons thrust were specifically targeted to determine whether a thermal signature is associated with the structure. Three graphitic schists were sampled, and all showed temperatures well above (387 °C to 459 °C) those away from the immediate vicinity of the Tons thrust (i.e., <330 °C; Fig. 4).

$^{40}Ar/^{39}Ar$ Thermochronology

In the preceding section, we documented temperatures in the Kumaun and Garwhal Lesser Himalayan Sequence up to ~560 °C. The cooling paths that these rocks have taken following metamorphism have the potential to provide additional insights into the tectonic development of the region. White micas associated with Himalayan metamorphism are particularly abundant near the Munsiari thrust and basal thrusts of the four klippen exposed to the north of the Tons thrust. Methods for these analyses are described in the GSA Data Repository (see footnote 1).

Figure 5 summarizes results of the $^{40}Ar/^{39}Ar$ study (see GSA Data Repository for full details [see footnote 1]). Calculated total fusion ages range between ca. 4 Ma and ca. 500 Ma. As with the pattern of the RSCM thermometric results, data are clustered across the study area, coinciding with areas where white mica is abundant. Lineation-forming white micas are most plentiful in the quartzites of the Berinag thrust hanging wall, and, as such, results are largely derived from this unit. South of the Tons thrust, rocks of the Main Boundary thrust and Ramgarh thrust hanging walls have metamorphic grades below those required to grow foliation-forming white mica, hence the lack of data from the *Outer* Lesser Himalayan Sequence.

In total, 33 white micas were analyzed by the $^{40}Ar/^{39}Ar$ step-heating method (Fig. 6). A wide range of gas release patterns is observed, which requires some interpretation. Within the somewhat chaotic range of age spectra (Fig. 6A),

three broad patterns emerge. The age spectra colored in blue are characterized by apparent ages younger than 20 Ma throughout more than 99% of gas release and small age gradients (typically ~3 Ma) over the gas release (typically 15 steps). This group of samples is referred to as mode 1 gas release pattern. Given the shape of gas release patterns for mode 1 samples, in combination with the observation that graphitic rocks adjacent to many of these samples have experienced peak temperatures >400 °C, mode 1 sample ages are interpreted as recording cooling through the closure temperature (T_c) for Ar diffusion in white mica of ~400 °C (Harrison et al., 2008).

Red age spectra (Fig. 6A) are typified by increasing apparent ages at each step, where the final 10% of gas release is yielded by older than 50 Ma ages. Gas release patterns typically yield Tertiary ages over ~70% of the gas release. This group of age spectra is referred to as mode 2. The rapid increases in age over the final 30% of gas release, in combination with incremental increases in age over the first 70%, suggest that mode 2 ages represent incomplete outgassing of detrital white micas rather than cooling ages. Evidence for this interpretation is provided by RSCM on rocks in proximity to mode 2 samples, which suggests that these rocks did not experience temperatures >350 °C.

A third group of samples (mode 3 gas release pattern) shown in green (Fig. 6A) consists of six samples with large analytical errors reflecting their low (0.2%–3%) potassium contents (i.e., the analyzed material is not pure muscovite). Because of the large errors associated with this group of analyses, samples displaying mode 3 gas release patterns are not considered further.

Figure 6B shows the combined age spectra of 16 samples characterized by mode 1 gas release. The range of calculated total fusion ages for these 16 samples varies between 13.5 Ma and 4.3 Ma (Fig. 6B). A broad pattern of younger total fusion ages with increasing proximity to the Munsiari thrust is observed. The oldest mode 1 age (GW168–04) is from a penetratively foliated Berinag quartzite in the southern footwall of the Askot klippe (Fig. 5), and the youngest age is from a kyanite-bearing Berinag quartzite (GW121–03A) of the Munsiari thrust's footwall, near the town of Munsiari. Along the length of the Munsiari thrust, mode 1 ages vary between 4.4 Ma and 10.4 Ma. In the central portion of the study area, apparent ages adjacent to the Munsiari thrust vary between 6 Ma and 10.4 Ma, averaging ca. 8.5 Ma. Along the Bhagirathi River, a single sample yielded a mode 1 release pattern with a total fusion age of 8.2 Ma, 3.2 km southwest of the Munsiari thrust. Four mode 1 ages from Lesser Himalayan Sequence rocks

in the footwall of the Main Central thrust sheet have been documented up to ~30 km south of the Munsiari thrust. Figure 5 shows that white micas separated from Berinag quartzites in the footwalls of the Chaukori and Askot klippen yield total fusion ages between 9.8 Ma and 13.6 Ma.

Figure 5 shows 12 mode 2 ages distributed across the Kumaun and Garwhal Lesser Himalayan Sequence. In the region's eastern and central parts, mode 2 release patterns have been documented from quartzites up to ~50 km south of the Munsiari thrust within the Berinag thrust's hanging wall. South of the Askot klippe, three samples were collected and analyzed with increasing distance from the klippe contact. The first two samples are characterized by mode 1 release, while the third (furthest from the klippe contact; GW170–04) shows mode 2 behavior. In the Garwhal region, eight mode 2 ages were recorded from the Berinag thrust's hanging wall in the vicinity of the Bhagirathi River. Calculated total fusion ages for these samples are interpreted to represent incomplete outgassing of detrital white mica at or below ~400 °C and not cooling through the white mica T_c.

Discussion of Thermal Data Sets

Results of the thermal study detailed here allow us to characterize and quantify the thermal structure of the Kumaun and Garwhal Lesser Himalaya along three broad transects. The distribution of thermal data is spatially variable and highly clustered in some areas, a reflection of the location and accessibility of suitable material for sampling.

In the case of the RSCM study (Fig. 4), note that south of the Tons thrust, all analyzed samples yield peak temperatures below the current limit of the technique of ~330 °C. On the northern side of the Tons thrust, 49 samples record a range of temperatures from <330 °C to 583 °C. Peak metamorphic temperatures immediately adjacent to the Munsiari thrust are typically ~550 °C, with a high of 571 °C recorded in far-east Kumaun. These results are consistent with those of Beyssac et al. (2004), who documented similar temperatures throughout the Lesser Himalayan Sequence of western and central Nepal at similar structural positions. Based on the aluminosilicate phase diagram (Holdaway, 1971; Kerrick, 1990), the presence of kyanite in quartzites (Fig. 3) adjacent to graphitic rocks that record peak metamorphic temperatures of ~550 °C constrains pressure in the quartzites to be ≥5 kbar.

The RSCM data detailed here point toward a spatial association between peak metamorphic temperatures and proximity to the hanging wall of the Main Central thrust (Fig. 4). Figure 4
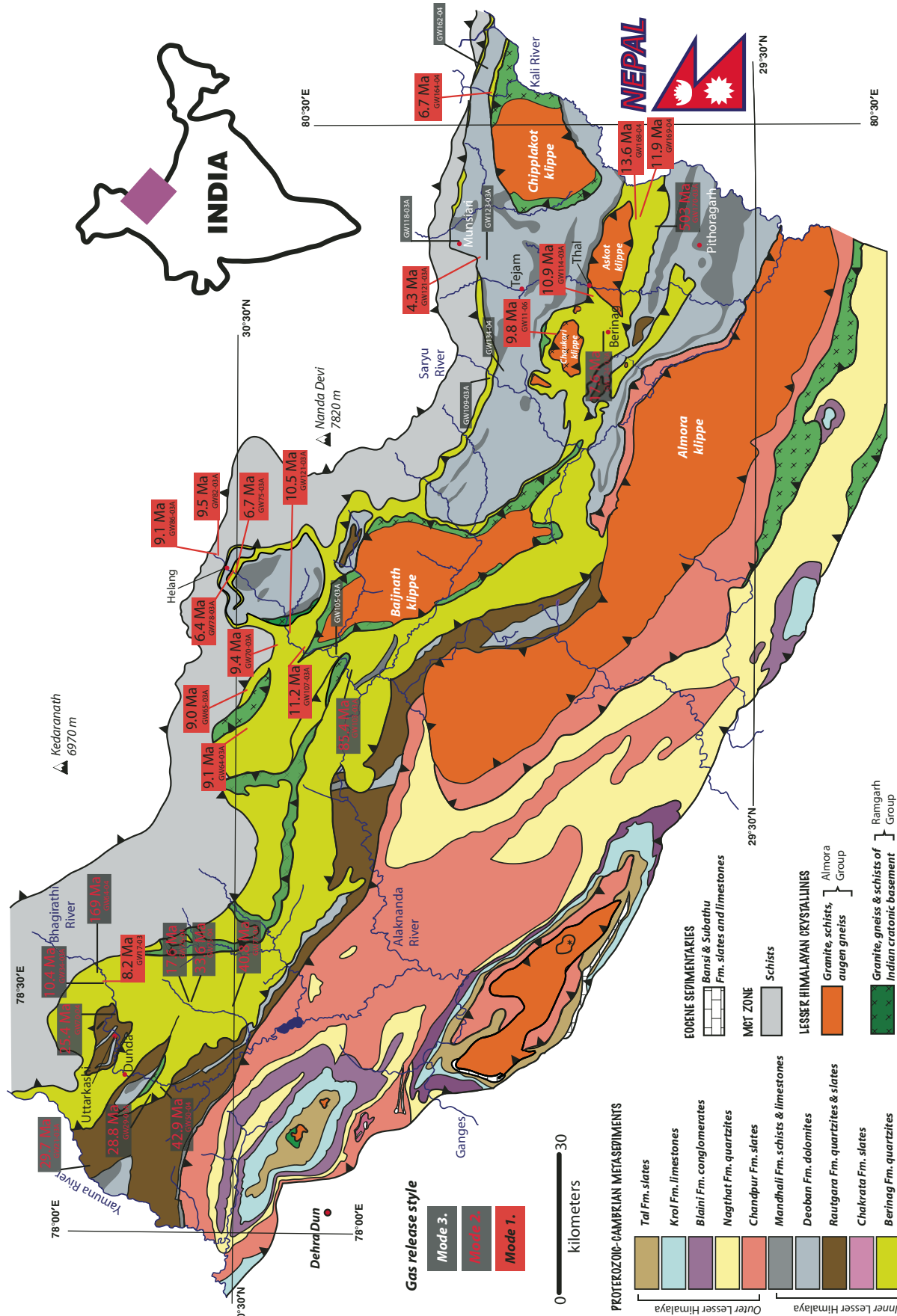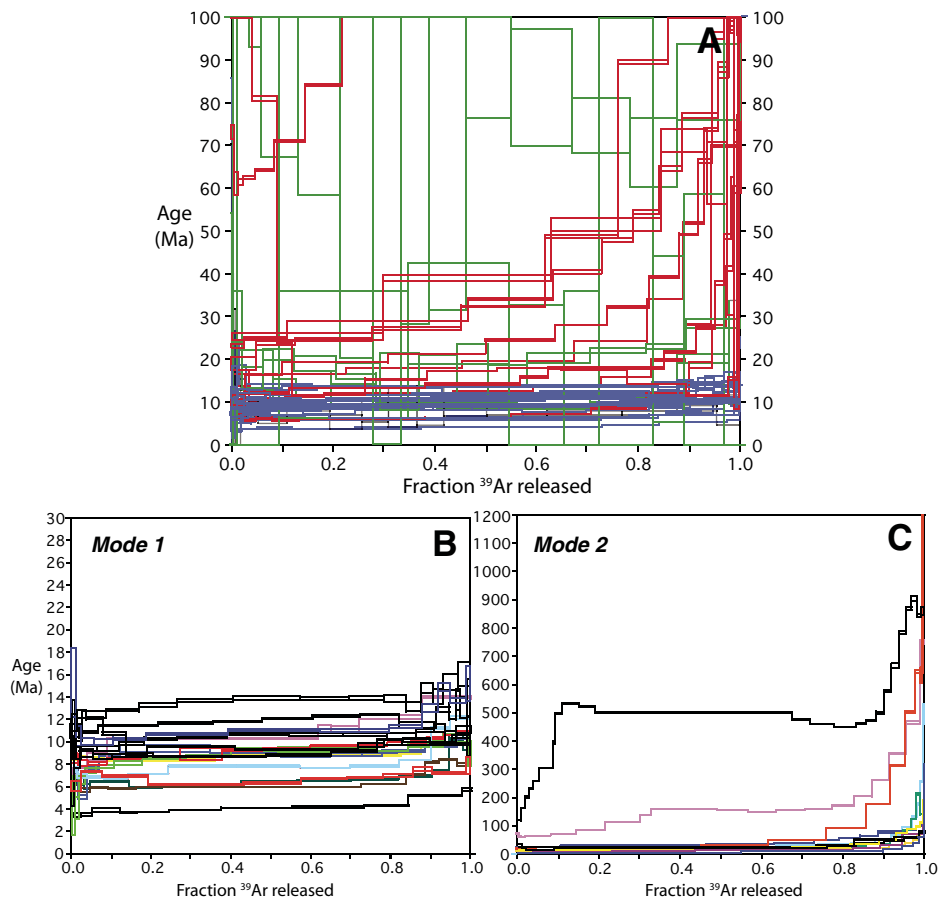
Kumaun and Garwhal Lesser Himalaya: Thermal and deformation histories

Figure 5. Geological map of the Kumaun and Garwhal Lesser Himalaya overlain with results of the ^{40}Ar/^{39}Ar thermochronological study of white mica.

Figure 6. ⁴⁰Ar/³⁹Ar age spectra for samples examined in the present study. (A) Combined
age spectra of 33 samples analyzed for this study. Mode 1 age spectra are blue, mode 2 age
spectra red, and mode 3 age spectra green. Lower portion of figure shows the age spectra
separated into mode 1 (B) and mode 2 (C) behavior. For mode 1 samples, note the shallowly
increasing age gradients between early and late steps of gas release. For the case of the mode
2 samples, note the roughly exponential increases in age in the final ~30% of gas release.

shows that *Inner* Lesser Himalayan rocks on the northern side of the Tons thrust display an increase in metamorphic temperatures as the Main Central thrust is approached (i.e., with higher structural position or shallower depth). This increase in metamorphic grade has long been recognized in Uttaranchal (Medicott, 1864; Middlemiss, 1887; Oldham, 1883), but it has not been previously quantified, nor has the magnitude of the inverted thermal field gradient beneath the Main Central thrust been estimated. In the previous results section, we qualitatively described the inverted metamorphic field gradient and RSCM thermometric data relative to the map distance to the Munsiari thrust. While it is a useful approximation, calculation of an inverted thermal field gradient based on map distance alone is potentially a gross oversimplification because it ignores the interplay between the complex structural geometry and differential erosion responsible for current exposure of the Lesser Himalayan Sequence.

Given that analyzed samples were not taken from a single section of common elevation, all data need to be collapsed to a common reference frame in order to compare results from different areas and accurately calculate thermal field gradients in the Lesser Himalayan Sequence. As the Main Central thrust is the boundary between the Lesser Himalayan Sequence and the Greater Himalayan Complex, it is the natural choice. However, the position of the Main Central thrust has been a matter of intense debate, and it reflects the varied criteria used to define its position: structural, lithologic, and chronostratigraphic (see discussion in Célérier et al., 2009).

The Main Central thrust has experienced an episodic history of displacement, and the current structural architecture in proximity to the fault reflects this extended sequence of fault-ing. LeFort (1996) showed that the large-scale displacements (hundreds of kilometers) responsible for juxtaposition of the Main Central thrust hanging wall atop the Lesser Himalayan Sequence occurred in the early Miocene and were associated with the MCT II (i.e., Vaikrita thrust). Collective displacements attributed to the Miocene-Pliocene, out-of-sequence phase of Main Central thrust thrusting are probably of significantly lower magnitude than the early Miocene phase of Main Central thrust activity (Harrison et al., 1997). So, the Main Central thrust–related structure of greatest tectonic significance appears to be the Vaikrita thrust (i.e., MCT II of Nepal), and therefore thermal field gradient calculations beneath the Main Central thrust have been referenced to it (i.e., perpendicular distance beneath the projected thrust plane). Figure 7 schematically represents the method for calculation of gradients. This approach considers the effect of differential elevations between analyzed samples and also approximates the first-order structural trends of the region.

Given the observation that metamorphic temperature peaks are spatially associated with proximity to klippen north of the Tons thrust, only samples unaffected by this relationship (i.e., distal to the klippen) are considered in the characterization of inverted metamorphism south of the Vaikrita thrust. Specifically, the suite of samples from the Gori Ganga River in far-eastern Kumaun and several samples from the Alaknanda River (Fig. 4) were excluded from the gradient calculation on this basis. This is to ensure that we are measuring the inverted thermal field gradient at the position of the Vaikrita thrust, and not including data from below more leading-edge positions of the Main Central thrust hanging wall. Eight samples were considered in the calculation, and these yield an inverted thermal field gradient of ~30 °C/km perpendicular to the Vaikrita thrust within the Lesser Himalayan Sequence (Fig. 7). This is consistent with the range of gradients documented by Beyssac et al. (2004) and Bollinger et al. (2004) beneath the Main Central thrust in Nepal.

In addition to the inverted thermal field gradients under the Vaikrita thrust, RSCM has revealed an inverted thermal field gradient in Lesser Himalayan Sequence rocks in the footwall of the Askot klippe in eastern Kumaun. This klippe sits atop the Lesser Himalayan Sequence ~25 km south of the trace of the Vaikrita thrust. On a southerly traverse from the Vaikrita thrust toward the klippe, recorded peak metamorphic temperatures fall to ~370 °C (near Tejam; see Fig. 4) before reaching a maximum of ~530 °C close to the fault at the base of the klippen (widely considered to be the southerly extension of the Vaikrita thrust).
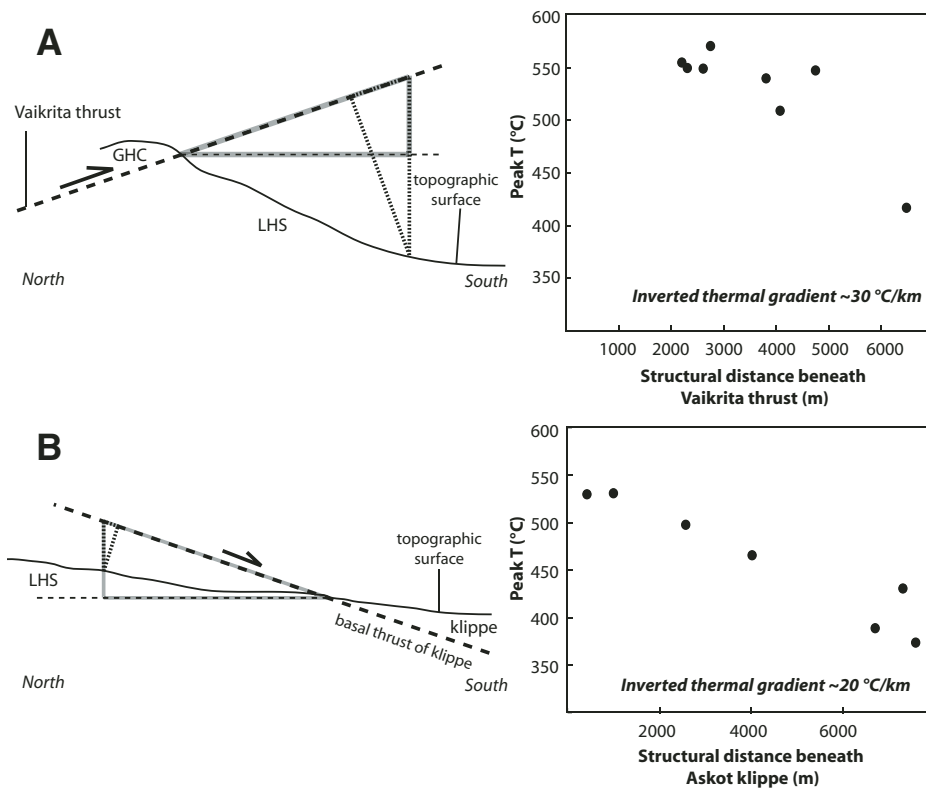
Figure 7. Details of thermal field gradient calculation for samples in the footwall of the Main Central thrust hanging wall. (A) The approach under the Vaikrita thrust. (B) The approach under the Askot klippe. Sketches on the left schematically represent the approach, while plots on the right show the calculated inverted thermal field gradients. GHC—Greater Himalayan Complex, LHS—Lesser Himalayan Sequence.

Uncertainties in identification of the structure to which inverted thermal field gradients may be referenced are avoided for the case beneath the Askot klippe because the boundary between the Main Central thrust hanging wall and footwall is sharp and readily identified on the basis of lithology (gneiss in the hanging wall and quartzite in the footwall). The inverted thermal field gradient (~20 °C/km) is lower than that beneath the Vaikrita thrust (Fig. 7).

Carbonaceous material was not found beneath the Almora klippe, precluding RSCM. However, turbidites immediately beneath the Almora klippe (Fig. 2) retain their sedimentary character. Spherical detrital quartz grains are preserved in the rock matrix, as are cross-beds in 10–20 cm sandstone horizons of the turbidite succession, indicating that rocks in the footwall of the Almora klippe did not experience temperatures >350 °C (Dunlap et al., 1997; Hirth and Tullis, 1992).

The spatial association between recorded temperature maxima in Lesser Himalayan Sequence rocks and proximity to the Main Central thrust hanging wall suggests a causal relationship, as does the inverted thermal field gradient beneath the Askot klippe, ~25 km south of the Munsiari thrust. The RSCM study also reveals a thermal field gradient in the footwall perpendicular to the strike of the Main Central thrust hanging wall, i.e., to the south. Peak metamorphic temperatures, and apparent inverted thermal field gradients, are highest beneath the Vaikrita thrust (550–560 °C, ~30 °C/km). However ~25 km south, at the position of the Askot klippe, peak temperatures are ~40 °C lower, and the inverted thermal field gradient is ~20 °C/km. Further south again, immediately below the Almora klippe, there does not appear to be any appreciable inverted thermal field gradient. If thermal excursions in the Lesser Himalayan Sequence are due to heat flow from the Main Central thrust hanging wall, then the southward decrease in the degree of Lesser Himalayan Sequence metamorphism, and associated inverted thermal field gradients, implies that the Greater Himalayan Crystalline unit cooled as it propagated south. At the position of the Askot klippe, sufficient heat was still available in the Main Central thrust hanging wall to heat the graphitic schists of the Lesser Himalayan Sequence to 530 °C. However, by the time the leading edge of the sheet reached approximately halfway between the traces of the Main Boundary thrust and the Vaikrita thrust, it had cooled below ~330 °C (i.e., quartz recrystallization and the lower limit of RSCM thermometry).

Three samples adjacent the Tons thrust record temperature excursions above that documented in rocks distal to the fault. These thermal anomalies support models for the assembly of the Himalaya that require a significant role for the Tons thrust (Ahmad et al., 2000; Richards et al., 2005).

The $^{40}Ar/^{39}Ar$ thermochronological results also point toward a spatial association between modes of sample degassing and proximity to the hanging wall of the Main Central thrust. Figure 5 shows that with increasing distance from the Main Central thrust hanging wall, age spectra shift from mode 1 to mode 2 behavior. Mode 1 cooling ages approach a minimum of 4.4 Ma near the type locality of the Munsiari thrust and a maximum of 13.6 Ma to the south, in the footwall of the Askot klippe. In the case of the four mode 1 ages recorded in the footwall of the Askot and Chaukori klippen (~50 km south of the Munsiari thrust, where Lesser Himalayan Sequence samples away from the klippen are characterized by mode 2 release patterns), the proximity of these cooling ages to the Main Central thrust hanging wall suggests that the elevated temperatures required to outgas detrital white micas and crystallize new grains were derived from the hot hanging wall of the Main Central thrust. This is consistent with the RSCM results, which also record increases in temperature approaching the Main Central thrust hanging wall. The cooling in the Main Central thrust footwall, recorded by $^{40}Ar/^{39}Ar$ white mica ages, also appears to be related to proximity to this fault. Thus, we interpret the $^{40}Ar/^{39}Ar$ ages of Lesser Himalayan Sequence white micas to reflect cooling below ~400 °C in the footwall of the Main Central thrust following emplacement of the Greater Himalayan Complex. Both data sets yield evidence to support this interpretation and indicate temperature excursions (spatially related to the Main Central thrust hanging wall) above the ambient temperature (<330 °C) of regional metamorphism in the Lesser Himalayan Sequence.

This interpretation implies that mode 1 ages are derived from rocks that were more proximal to the heat source of the Greater Himalayan Complex, and therefore experienced greater heating, than mode 2 samples. The partial resetting of mode 2 white micas suggests that they record a Tertiary thermal event at conditions close to the white mica T_c but insufficient to fully

outgas accumulated $^{40}Ar^*$ from the Proterozoic-age detrital white micas. Thus, Tertiary ages in the early steps of gas release from these samples may not be related to cooling through T_c, but, rather, they may relate to the time of crystallization of low-retentivity white mica during Himalayan tectonism (Dunlap, 1997). If so, an estimate of the minimum age of crystallization of the mode 2 samples, and thus the timing of passage of the Main Central thrust hanging wall over the Lesser Himalayan Sequence, can be obtained by considering the calculated age for a given sample at the first step of gas release.

Our interpretation of mode 1 $^{40}Ar/^{39}Ar$ ages is that they represent cooling through the closure temperature for muscovite. We estimate the bulk muscovite T_c to be 400 °C based on the Arrhenius parameters of Harrison et al. (2009) and an effective diffusion length scale of 0.005 cm.

Mode 1 cooling ages are characterized by gas release patterns exhibiting an age gradient between the early and late stages of step heating, typically ~3 Ma (Fig. 6). An implication of our ability to reveal intracrystalline diffusion gradients in white micas during in vacuo step heating is that $^{40}Ar/^{39}Ar$ age spectra of natural materials can reveal cooling-related age gradients. This observation is consistent with many other studies documented in the literature (see McDougall and Harrison, 1999). If so, we can obtain an estimate of cooling rate from the expression for T_c as a function of position in a crystal of infinite cylinder geometry (Dodson, 1986). For the muscovite parameters described here, the T_c at the center of the cylinder (i.e., $r = 0.0$) is 410 °C. The same calculation for $r = 0.99$ yields an expected lower T_c of 320 °C. Given that the age difference across the release patterns averages ~3 Ma (Fig. 6), this 90 °C difference corresponds to a cooling rate of ~30 °C/Ma.

The difference of ~3 Ma between the first and last steps in an age spectra means that samples that record total fusion ages that are different by millions of years may actually have gas release steps that overlap in age. For example, calculated total fusion for samples GW114–03A and GW64–03A (see Data Repository material [see footnote 1]) differ by 2 Ma, yet the final 30% of gas release from the younger GW64–03A overlaps in age with the first 30% gas release from the older GW114–03A. So, following the reasoning of the previous paragraph, total fusion ages of ca. 6 Ma to ca. 11 Ma adjacent to the Munsiari thrust likely represent an average age of cooling at this structural level of 8.5 Ma. Thus, we conclude that the footwall of the Munsiari thrust across Uttaranchal experienced cooling below the T_c for white mica at ca. 8.5 Ma. A single sample from the type location of the Munsiari thrust falls outside this age

range. This sample, collected from an equivalent structural level to the ca. 8.5 Ma group, records a total fusion age ~4 Ma younger than the nine samples of structural equivalence.

South of the Munsiari thrust, a second group of samples exhibit mode 1 gas release patterns. In the footwalls of the Chaukori and Askot klippen, four samples are characterized by gas release patterns showing age gradients. In a similar manner to mode 1 samples adjacent to the Munsiari thrust, these samples display an ~3 Ma age gradient, which we interpret as intracrystalline closure profiles (Dodson, 1986). Calculated total fusion ages for these samples between 9.8 Ma and 13.6 Ma are significantly older than mode 1 ages adjacent to the Munsiari thrust. The average age of this group of samples from the footwall of the Askot and Chaukori klippen is 11.5 Ma, ~3 Ma older than samples in the footwall of the Munsiari thrust. The implication of the age differences in mode 1 samples from northern and southern exposures is that the southerly results document cooling of the Lesser Himalayan Sequence related to passage of the Main Central thrust hanging wall ~3 Ma before the samples to the north.

The ~3 Ma separation in mode 1 ages between northerly and southerly exposures of the Main Central thrust footwall interface requires a mechanism to account for this contrast. By way of explanation, we consider the thermal consequences of faulting along the Main Central thrust. In its simplest form, the thermal relation-ship between the Main Central thrust hanging wall and footwall is one of juxtaposition of a hot upper plate against a colder lower plate. Thermal metamorphism in the footwall occurs principally via heat conduction below the fault interface. Following the cessation of movement along the fault, the perturbed isotherms will tend toward equilibrium. In order to produce the observed temperature maxima beneath the klippen, thrusting and accompanying isotherm displacement would need to be of sufficient magnitude to produce a sigmoidal-shaped isotherm pattern along the thrust interface that relaxes over time (Fig. 8). Two-dimensional modeling of pressure-temperature-time (*P-T-t*) paths for regional metamorphism in overthrust terrains (Shi and Wang, 1987) has shown that the leading edge of the overriding thrust sheet will be cooler than the root, and that it cools much more rapidly than near the root. Following cessation of thrusting, the trend is one of fast cooling at the thrust sheet's leading edge and maintenance of elevated temperatures in the root zone. Further, the rapid cooling at the leading edge slows as the cooling front migrates toward the hotter root zone of the thrust sheet. Allowed to proceed to equilibrium, the result is elimination of the sigmoidal isotherm structure, where the thrust sheet root zone is the last to cool (Fig. 8). We propose that the pattern of younger mode 1 cooling ages with increasing proximity to the Munsiari thrust is a reflection of this mechanism. The ca. 11 Ma cooling age at the position of the Chaukori and
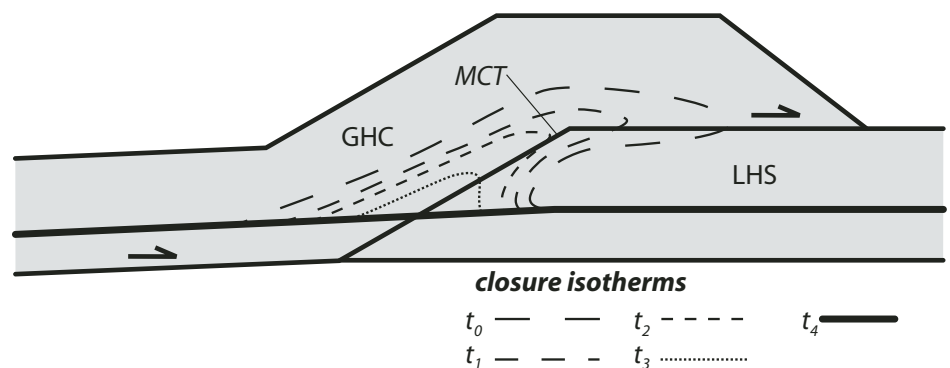
Figure 8. Schematic illustration of isotherm relaxation following the cessation of thrusting along a simple ramp flat; t_0 represents the sigmoidal isotherm pattern produced immediately after thrusting ceases, and t_1–t_4 show the retreating closure isotherm for white mica migrating toward the thrust root zone. Shi and Wang (1987) showed that following the cessation of thrusting, the leading edge of the overthrust terrain cools quickly and then slows as the perturbed isotherms retreat toward the hotter root zone, until the thermal anomaly is dissipated at t_4. In this study, the pattern of older mode 1 ages in the south of the Lesser Himalayan Sequence (LHS) and younger mode 1 ages to the north is explained through such a mechanism—retreat of isotherms, and subsequent cooling in the Main Central thrust (MCT) footwall, following the emplacement of the Greater Himalayan Complex (GHC) hanging wall upon the Lesser Himalayan Sequence.

Askot klippen records the time that the thermal anomaly attributed to emplacement of the Main Central thrust hanging wall dropped below the T_c for muscovite. Samples from the more northerly Munsiari thrust hanging wall are closer to the root zone and so cooled later (and recorded younger cooling ages) than samples closer to the thrust sheet's leading edge (Fig. 8) as a result of the retreat of the white mica closure isotherm toward thermal equilibrium.

THERMO-KINEMATIC MODELING

The data sets detailed herein provide constraints on the thermo-tectonic evolution of the Kumaun and Garwhal Lesser Himalayan Sequence. Taken individually, each of these data sets constrains singular aspects of the assembly of the studied area. However, the combination of these results within the framework of a multiparameter physical model has the potential to quantitatively test tectonic hypotheses. Accordingly, we used numerical experiments to investigate the thermal response of the Lesser Himalayan Sequence to juxtaposition of a hot upper plate. This style of model has been proposed by multiple Himalayan workers over the past 30 a, beginning with LeFort (1975). Known as the "hot-iron" model, this hypothesis was the first to present a testable physical mechanism for Himalayan inverted metamorphism. A suite of publications (e.g., Shi and Wang, 1987; Ruppel and Hodges, 1994) quantitatively assessed the Le Fort (1975) proposition and showed that, under realistic fault slip rates, inverted metamorphism could not be achieved through thermal relaxation following thrusting alone. Furthermore, a key requirement of these models is that, in order to obtain the required high temperatures to metamorphose the Main Central thrust footwall, an extraordinary heat source in the Main Central thrust hanging wall is necessary to counter the refrigeration effect of conductive cooling to the footwall. Preempting this limitation, Le Fort (1975) invoked shear heating along the Main Central thrust as a potential source of the required heat. A series of papers subsequently addressed Le Fort's (1975) proposition quantitatively (Graham and England, 1976; England et al., 1992; England and Molnar, 1993; Molnar and England, 1990). These studies successfully reproduced aspects of the observed thermal structure, but only by using shear stresses in the range of 100–1100 MPa. Despite reproducing the inferred Himalayan thermal structure, the applicability of these models was diminished by the extraordinary magnitude of required shear stresses. Paleopeizometric (Engelder, 1983), laboratory deformation (Rutter, 1997), and tec-

tonic modeling studies (Kong and Bird, 1996) are consistent with ductile shearing stresses of ≤50 MPa (Harrison et al., 1999).

In addition to modeling a "hot-iron" style scenario, we also modeled the thermal effects of duplex formation in the Lesser Himalayan Sequence following an early phase of Greater Himalayan Complex juxtaposition against the Lesser Himalayan Sequence along the Main Central thrust. This is consistent with kinematic models of Lesser Himalayan Sequence assembly proposed by workers in Nepal (Schelling and Arita, 1991; DeCelles et al., 2001; Robinson et al., 2003, 2006; Bollinger et al., 2004, 2006), as well as with the structural geology of the study area documented in Célérier et al. (2009).

To represent the thermal conditions of the study area, a successful model of the Lesser Himalayan Sequence should account for the following constraints:

(1) temperature of regional low-grade metamorphism <330 °C;

(2) localized temperature maxima up to 550–570 °C immediately adjacent the Main Central thrust;

(3) apparent inverted thermal field gradients (~30 °C/km normal to the base of the Main Central thrust) adjacent to the Main Central thrust with a mean maximum temperature of ~550 °C at the contact;

(4) temperatures and inverted thermal field gradients highest at the base of the high range; peak temperatures ~40 °C lower and inverted gradient of ~20 °C/km 25 km south (i.e., Askot klippe footwall), and a further 25 km south (i.e., Almora klippe footwall), no inverted gradient observed;

(5) mode 1 ^{40}Ar/^{39}Ar white mica ages indicating Lesser Himalayan Sequence cooling below ~400 °C from 13.6 to 4 Ma, where ages adjacent the Main Central thrust reflect cooling following Greater Himalayan Complex emplacement, and the Main Boundary, Tons, and Berinag thrusts do not appear to have influenced closure of the white mica ^{40}Ar/^{39}Ar chronometer; and

(6) average mode 1 ^{40}Ar/^{39}Ar white mica ages adjacent the Main Central thrust in the Chaukori and Askot klippen of ca. 11.5 Ma (i.e., ~3 Ma older than at the base of the high range).

Modeling Approach

To investigate the thermal evolution of the study area, we employed a highly flexible thermo-kinematic numerical model. Our intention here is not to search for parameters that provide an exact fit to the data, but rather to test whether a proposed hypothesis is broadly consistent with predictions of thermo-kinematic modeling.

Thermo-kinematic Model: PECUBE

We solve the heat-transfer equation in two dimensions:

$$\rho c \left(\frac{\partial T}{\partial t} + v \nabla T \right) = k \nabla^2 T + \rho H + H_s \quad (1)$$

where $T(x,y,z,t)$ is the temperature (K), ρ is rock density (kg/m^3), c is heat capacity (J/kg K), $v(u,v,w)$ is the velocity field (km/Ma), k is the thermal conductivity (Wm/K), $H(x,y,z)$ is radioactive heat production per unit mass (μW/m^3), and H_s is the shear heating (J/a). We use a modified version of a finite-element code (PECUBE; Braun, 2003; Herman et al., 2007) to solve Equation 1 within a crustal block, including the effects of a time-varying topography. The effects of radiogenic heat production and shear heating are included. Shear heating is computed as the product of the shear stress and strain rate tensors (e.g., Graham and England, 1976; England et al., 1992; Burg and Gerya, 2005). The strain rate can be estimated from the velocity field, whereas the components of the stress tensor can only be approximated, since the model is kinematic. In the brittle domain, all the components of the stress tensor are taken equal to the lithostatic pressure ($\tau = \mu[\rho - \rho_w]gz$ and $\mu = \tan[\phi]$, where τ is the shear stress [Pa], g is the gravitational acceleration [ms^{-2}], ρ_w is the density of water, z is the depth [m], and ϕ is the friction angle). In the ductile domain, the shear stress is calculated from a power law, $\tau^n = \dot{\varepsilon}/(A^{-Q/RT})$ where $\dot{\varepsilon}$ is the strain rate (1/Ma), n and A (1/MPa s) are intrinsic constants, Q (J/mol) is the activation energy, and R is the universal gas constant. A granite flow law is used for the parameters in the ductile regime, and a 50 MPa value is assumed for the maximum shear stress, in line with the range of values consistent with laboratory experiments (Hansen and Carter, 1982).

At the end of the model run, we extract thermal histories to estimate ages and peak temperatures for rocks that end up at the surface. The thermochronological ages are computed by solving the solid-state diffusion equation, as described in Herman et al. (2007), using the kinetic parameters from Harrison et al. (2008). Our goal is to reproduce the horizontal variations in age and peak temperature that dominate age patterns in the data.

Model Kinematics

Figure 9 schematically shows the kinematics of the model. We assume a two-stage kinematic evolution. In the first stage (Fig. 9A), we simulate the effect of an overthrusting hot hanging wall over a downgoing footwall ("hot-iron" style thermal effect) within a crustal block that

A

North   South

B

ZONE OF HIGH
EXHUMATION/ROCK UPLIFT

North   South

ZONE OF
UNDERPLATING
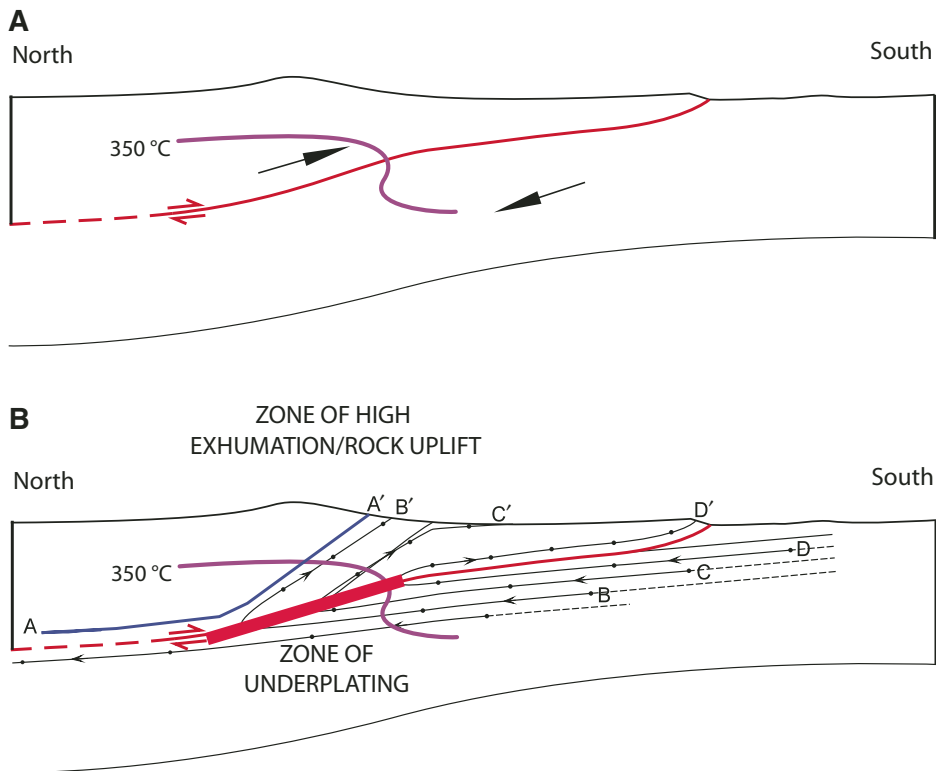
Figure 9. Sketch of the kinematics used in PECUBE (modified from Avouac, 2008). (A) First stage of the model ($t \leq t_e$). (B) Second stage of the model includes underplating ($t \geq t_e$).

is 200 km long and 60 km thick. The main thrust is treated as a flat ramp, defined in the model by a kink-fault, which is assumed to be equivalent to the Main Himalayan thrust. The velocity field is defined according to the fault-bend fold method (Suppe, 1983). The location of the kink is imposed at depth of 11 km and 70 km north from the trace of the thrust at the surface (Cattin and Avouac, 2000; Lavé and Avouac, 2000, 2001). The dip of the ramp is set equal to 15°, consistent with Cattin and Avouac (2000) and Lavé and Avouac (2000, 2001). The displacement along this thrust is achieved by ascribing a total convergence velocity, $v_t = 20$ mm/a, consistent with estimates of Himalayan convergence (Armijo et al., 1986; Avouac, 2003; Bilham et al., 1997; Bettinelli et al., 2006) that is partitioned between the footwall (underthrusting) and hanging wall (overthrusting) velocities, v_u and v_o, respectively (i.e., $v_o = [1 - \lambda]v_t$ and $v_u = \lambda v_t$). The overthrusting rate is related to the erosion rate such that when the overthrusting rate is increased, increased erosion results. We are able to constrain λ because we are able to constrain the erosion rate. This initial stage of model development is intended to reproduce the effects of large-scale displacement along the Main Central thrust responsible for juxtaposition of the Main Central thrust hanging

wall atop the Lesser Himalayan Sequence, as documented by LeFort (1975, 1996). During this first stage ($t < t_e$; Fig. 9A), some accretion (E_a [mm/a]) is included all along the thrust. In the second stage of the model ($t > t_e$, Fig. 9B), we aim to include the effects of duplex formation in the Lesser Himalayan Sequence as discussed previously here and in detail in Célérier et al. (2009). To achieve this, we increase the total vertical exhumation (E_u [mm/a]) over a given window lying between a distance 85 and 130 km away from the trace of the Main Himalayan thrust at the surface (Cattin and Avouac, 2000; Lavé and Avouac, 2000, 2001; Bollinger et al., 2004, 2006). This zone of vertical exhumation, in turn, corresponds to a local increase of erosion in the vicinity of the model's Main Central thrust trace. It is important to realize that as we add this vertical exhumation, material from the underthrusted plate is transferred through the main thrust, which allows us to explain the observed inverted metamorphic gradient as well as the formation of a duplex structure similar to those previously described by Schelling and Arita (1991), DeCelles et al. (2001), Robinson et al. (2003, 2006), Bollinger et al. (2004, 2006), and Célérier et al. (2009). This is illustrated in Figure 9B, where rock B, C, and D are underthrust below the Main Himalayan thrust, underplated, and ex-

posed at the surface in B′, C′, and D′. During this second stage, we can accurately track the evolution of a sheet lying above the Main Himalayan thrust, given as the boundary between two, oppositely verging rock sheets (Fig. 10). The trace of the exposed thrust sheet (black dots, Fig. 10) at the end of the numerical experiment is then used to define the location and dip of the Main Central thrust (Fig. 10B).

Model Results and Implications

In Figures 10A and 10B, we show the simulated thermal field with the crustal block at the beginning and at the end of the simulation, respectively. The numerical experiments were conducted for an equivalent duration of 35 Ma. The model includes a large number of parameters controlling both the physical properties of the crust and the geometry of the numerical experiment, all of which were adjusted by trial and error to fit the data. Preferred values are summarized in Table 2. We report here a limited number of model runs (model 1–4) with the objective of first showing that the chosen kinematics lead to a good fit to the data and then illustrating the effects of (1) partitioning between underthrusting and overthrusting, (2) the underplating rate through E_u, and (3) the timing of duplex formation.

In Figures 11 and 12, we compare model predictions to actual data. Figure 11 depicts horizontal distance versus $^{40}Ar/^{39}Ar$ muscovite age, whereas Figure 12 shows structural distance below the Main Central thrust versus peak temperature below the Vaikrita thrust (Figs. 12A and 12B). Model 1 corresponds to a case that leads to a reasonable fit to the data. For this model, λ is set equal to 0.75, t_e is 10 Ma, and E_u is 1.65. It clearly shows that the tectonic model allows us to fit both the $^{40}Ar/^{39}Ar$ muscovite ages and peak temperatures constrained by RSCM. The peak temperatures provide constraints on the thermal field along and near the Main Central thrust, whereas the $^{40}Ar/^{39}Ar$ muscovite ages constrain the subsequent cooling. In model 2, we change t_e to 15 Ma and keep E_u at 1.65 to ensure that the simulated Main Central thrust ends up at the same distance from the trace of the Main Himalayan thrust. It appears that it does not substantially affect the fit to the data. In models 3 and 4, we now increase and decrease λ to 0.85 and 0.5, respectively, which decreases and increases the erosion rate, since topography is fixed in the model. This has a dramatic effect on the model predictions. In the case where we decrease the overthrusting rate (model 3), it leads to a more pronounced cooling of the upper crust and in turn older ages and lower peak temperature at the surface. In the opposite
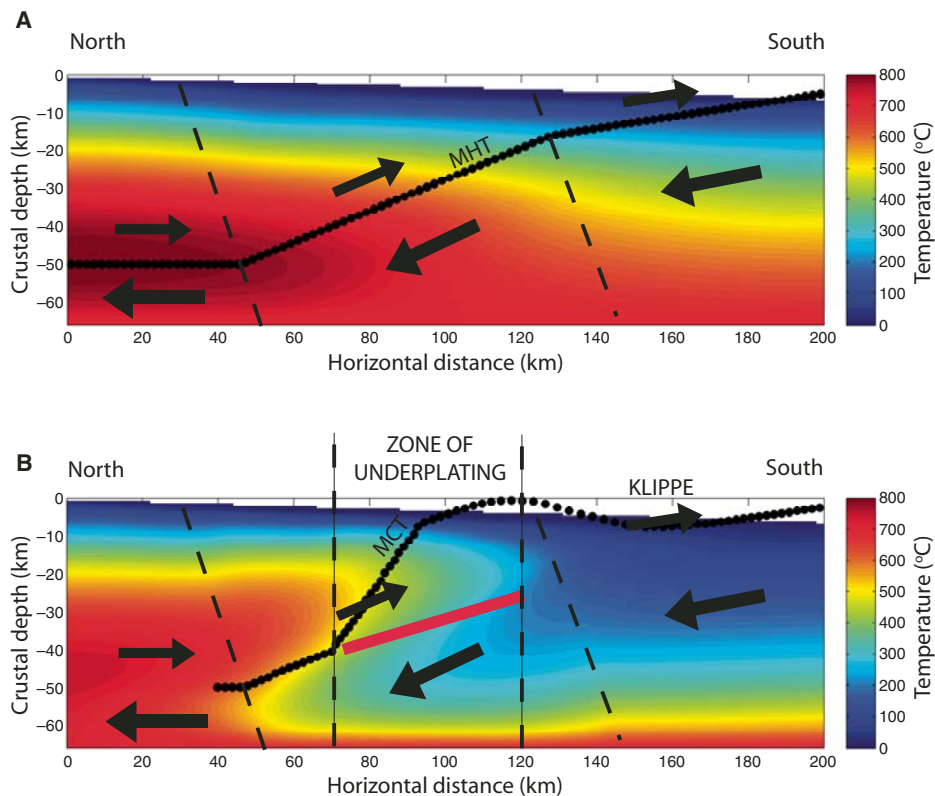
Figure 10. Thermo-kinematic model. (A) Example of thermal field at the beginning of simulation. (B) Example of thermal field at the end of the simulation. The black dots mark the position of the modeled Main Himalayan thrust (MHT)—the boundary between two, oppositely verging, rock sheets—and graphically represent how the Main Central thrust (MCT) evolves. The black arrows show the velocity field on either side of the Main Himalayan thrust. The region of enhanced exhumation/underplating since time equal t_e is highlighted in pink in part B.

scenario, the system is hotter, and the ages are younger. The models illustrate that the thermal structure of the Lesser Himalayan Sequence is most sensitive to the kinematic history (i.e., rate of overthrusting versus underthrusting along the Main Himalayan thrust) and that parameters such as heat production and heat conductivity are of lesser importance. The results are comparable to observations made in central Nepal, as described in Avouac (2008).

Existing models for the assembly of the Himalaya are based upon petrologic and thermochronologic data derived almost exclusively from the Greater Himalayan Complex, but which have been used nonetheless to make predictions for the *P-T-t* evolution of the Lesser Himalayan Sequence. The data presented here (in the case of the cooling age data, the first of their kind from the footwall of the Main Central thrust) provide a unique opportunity to test the predictions made by these models regarding the thermal character of the Lesser Himalayan Sequence. Currently, models for the assembly of

the Lesser Himalaya fall into three categories. (1) Thermal-mechanical models examine the evolution of the Lesser Himalayan Sequence within the larger context of the Himalaya-Tibet orogenic system. These are typified by the works Beaumont et al. (2001, 2004), Harrison et al. (1998), and Jamieson et al. (2004). In this group, the data used to constrain model evolution are predominantly derived from the Greater Himalayan Complex. Despite this, these models make specific predictions for the *P-T-t* evolution of the Lesser Himalayan Sequence. (2) A second group of thermal-kinematic models addresses the evolution of the Lesser Himalayan Sequence by focusing the modeling effort on the Lesser Himalayan Sequence. The works of Bollinger et al. (2004, 2006) use petrologic and thermochronologic constraints derived from the Greater Himalayan Complex and Lesser Himalayan Sequence to interrogate the tectonics responsible for Lesser Himalayan Sequence construction in Nepal. (3) Qualitative kinematic models target the construction of the Lesser

Himalayan Sequence, some of which are based upon quantitative petrologic and thermochronologic constraints from the Lesser Himalayan Sequence, some of which are not. This group of models includes DeCelles et al. (2001) and Robinson et al. (2003). The thermal data presented here allow us to assess the suitability of the predictions made by these models to the evolution of the Lesser Himalayan Sequence.

In the "channel-flow" model (Beaumont et al., 2001, 2004; Jamieson et al., 2004), *P-T-t* paths for Lesser Himalayan Sequence rocks were proposed. Jamieson et al. (2004) attributed the *P-T-t* evolution of the Lesser Himalayan Sequence to burial beneath a high-temperature region ahead of an advancing channel of Greater Himalayan Crystalline rocks. *P-T-t* histories were calculated for four model points assigned as representative of the Lesser Himalayan Sequence. A range of predicted peak temperatures for these points varied between $T_{max} = 285$ °C and $T_{max} = 735$ °C, where some rocks entered the sillimanite stability field. An examination of these *P-T-t* conditions in light of the RSCM data shows that the lower bound calculation is within the range of results presented herein. However, the $T_{max} = 735$ °C is ~150 °C hotter than the hottest measured RSCM data point in the Kumaun and Garwhal Lesser Himalayan Sequence, precluding this feature of their model. In Jamieson et al. (2004), rapid cooling of the Lesser Himalayan Sequence in the final 5–8 Ma of model evolution accompanies rapid exhumation by thrusting and erosion below the Main Central thrust as the model orogen propagates into its foreland. The cooling ages presented here indicate that cooling of the Lesser Himalayan Sequence commenced ~5 Ma before that proposed in the Jamieson et al. (2004) model. In addition, $^{40}Ar/^{39}Ar$ data presented here document a gradient in Lesser Himalayan Sequence cooling between 13.5 Ma and 8 Ma. The cooling ages therefore do not support the proposition of Jamieson et al. (2004) that rapid, uniform Lesser Himalayan Sequence cooling and exhumation are attributable to thrusting in the Lesser Himalayan Sequence between 5 and 8 Ma.
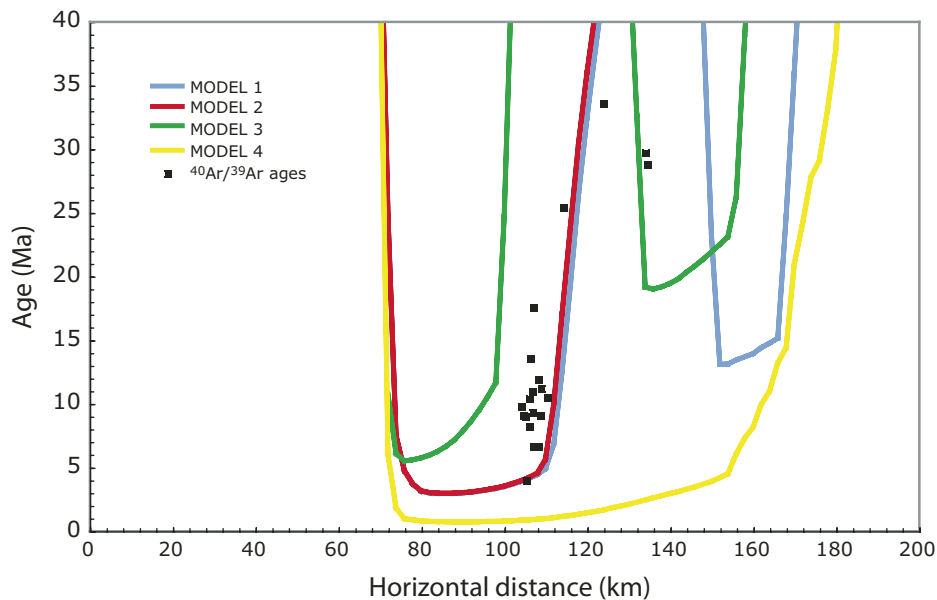
Figure 11. Modeling results. Model prediction compared to measured ⁴⁰Ar/³⁹Ar muscovite ages.

Harrison et al. (1998) used constraints from the ages of Miocene granite crystallization, the age of Main Central thrust zone recrystallization, and mineral age patterns from the Greater Himalayan Complex to constrain a thermal-kinematic model of the Himalayan orogen. In their model, they imposed a ramp-flat geometry to the Himalayan thrust system and ascribed slip to a number of faults conceived to represent the Himalayan thrust system, Main Central thrust, Main Boundary thrust, Main Central thrust zone, and Main Frontal thrust over 25 Ma of model time. Modeled geological phenomena relevant to the Lesser Himalayan Sequence were produced by a period of slip along the Main Central thrust between 25 and 15 Ma followed by an out-of-sequence phase of Main Central thrust zone slip between 8 and 2 Ma. Inverted metamorphic sequences of the Main Central thrust zone were generated through reactivation of the Main Central thrust (in the Main Central thrust zone), which caused subduction of Lesser Himalayan Sequence rocks to 25 km depth, where they reached 550 °C before being accreted to the upward-moving Main Central thrust hanging wall at ca. 6 Ma. The episodic slip history of the Main Central thrust in their model is somewhat inconsistent with the ⁴⁰Ar/³⁹Ar cooling ages presented here from the Main Central thrust footwall. Importantly, the results generated in this study define a gradient in cooling ages within the Main Central thrust footwall. Models presented here relate this gradient in ages to thermal relaxation following emplacement of the Main Central

thrust hanging wall atop the Lesser Himalayan Sequence. Episodic, out-of-sequence activity on the Main Central thrust would be reflected by sharp boundaries in the cooling ages, contrary to the gradient in ages observed.

The second class of models for evolution of the Lesser Himalayan Sequence uses ⁴⁰Ar/³⁹Ar age data as well as RSCM data from western and central Nepal to construct numerical simulations of Lesser Himalayan Sequence development. In the models of Bollinger et al. (2004, 2006), the thermal structure of the Nepal Himalaya is reproduced in a scenario of continuous slip along the Main Himalayan thrust over 20 Ma and growth of the Himalayan wedge resulting from underplating, which leads to duplex formation at midcrustal depth. The position of the 70-km-wide accretion window and the rate of underplating determine the gradient of peak metamorphic temperatures as well as the geometry of the underplated body. In these models, the inverted thermal field gradients documented by Beyssac et al. (2004) are successfully reproduced, as well as a pattern of ⁴⁰Ar/³⁹Ar cooling ages from the Main Central thrust hanging wall, but the success of the model in doing so is dependent on the accretionary window spanning a range of temperatures between 320 °C and 550 °C. The inverted thermal field gradients documented in this study are of similar magnitude to those used in these models and so support the findings of these simulations.

The final class of models that can be assessed in light of the thermal data presented here includes the qualitative kinematic models

of DeCelles et al. (2001) and Robinson et al. (2003). In these models, inverted thermal field gradients in the Lesser Himalayan Sequence result from structural imbrication, i.e., successive incorporation of Lesser Himalayan Sequence thrust sheets into a duplex, which is fed from the Main Himalayan thrust. The gentle northward dip of the Main Himalayan thrust and the northward increase in topographic overburden result in gradually northward-increasing conditions of metamorphism. The RSCM data presented in this study, as well as in Beyssac et al. (2004), demonstrate that inverted metamorphic gradients in the Lesser Himalayan Sequence are not gradual but steep, up to ~40 °C/km. DeCelles et al. (2001) and Robinson et al.'s (2003) mechanism for inverted thermal field gradients in the Lesser Himalayan Sequence are therefore not supported by the thermometric data in this study. Robinson et al. (2003) proposed that late Miocene to Pliocene ages from the lower, trailing part of the Greater Himalayan Complex and underlying Lesser Himalayan Sequence result from exhumation accompanying movement of thrust sheets of a Lesser Himalayan duplex over the main footwall ramp beneath a duplex. Details of this mechanism are not provided, but the general pattern of ⁴⁰Ar/³⁹Ar cooling ages presented here neither supports nor refutes this aspect of these models.

CONCLUSION

Our understanding of the geologic evolution of the Himalaya has been limited by a lack of quantitative constraints on the thermal evolution of the orogen outside the Greater Himalayan Complex. We have undertaken an integrated field, geochemical, and numerical modeling investigation to provide quantitative constraints on the structural and thermal evolution of the Lesser Himalayan Sequence in the Uttaranchal region of India.

The thermal structure of the Kumaun and Garwhal Lesser Himalaya was investigated using Raman spectroscopy of carbonaceous material (RSCM) and ⁴⁰Ar/³⁹Ar thermochronology. The RSCM study shows that the Kumaun and Garwhal Lesser Himalaya have experienced locally variable thermal metamorphism. South of the Tons thrust, peak metamorphic temperatures are below the current limit of the RSCM technique (~330 °C). However, on the northern side of the Tons thrust, a transition to higher temperatures adjacent to the Main Central thrust hanging wall is documented, with peak temperatures up to ~570 °C recorded. In the immediate footwall of the Main Central thrust, peak measured temperatures average ~550 °C. We quantified the long-recognized
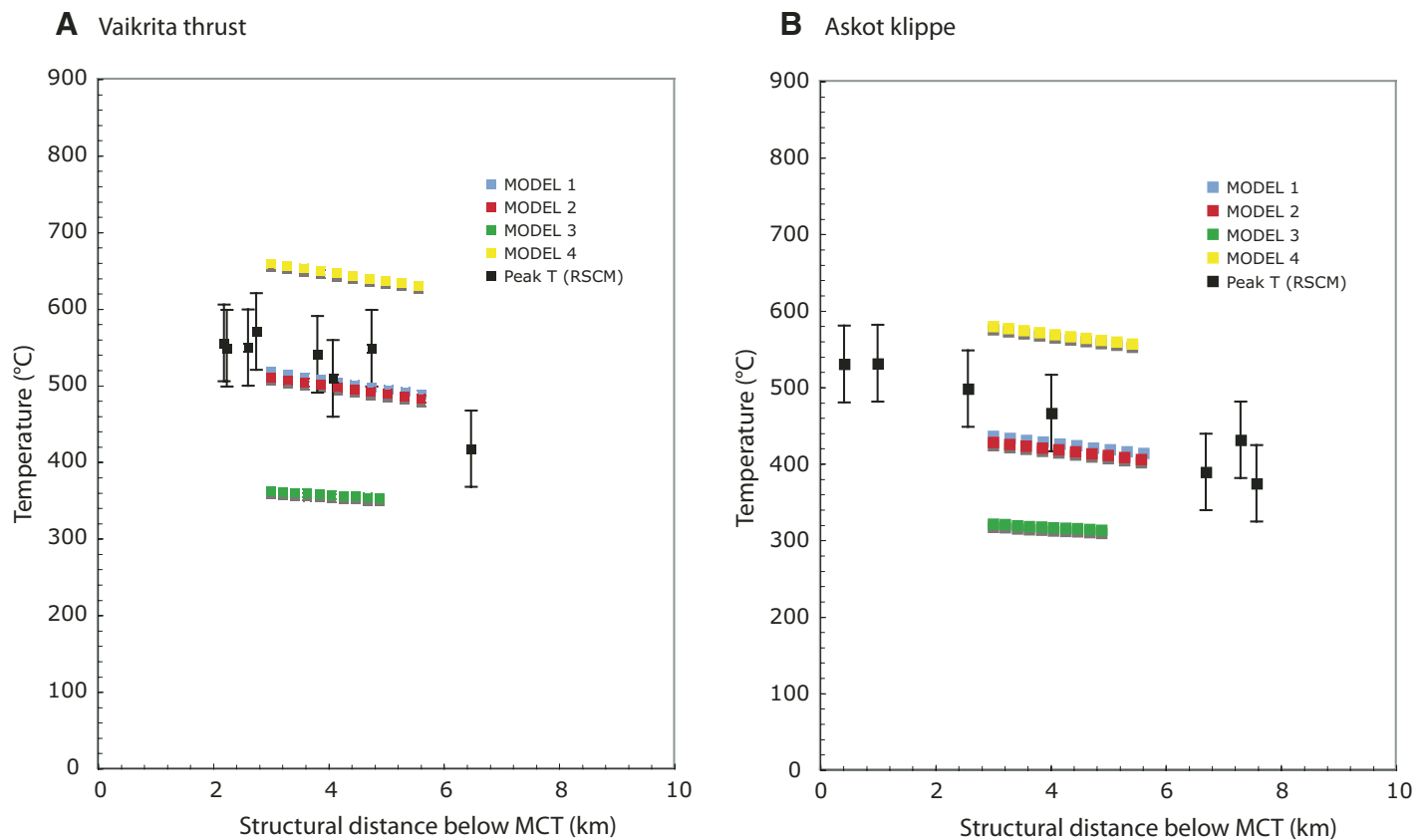
Figure 12. Modeling results. Model prediction compared to measured peak temperatures estimated from Raman spectroscopy of carbonaceous material (RSCM). (A) Vaikrita thrust. (B) Askot klippe. MCT—Main Central thrust.

inverted thermal field gradient in the Lesser Himalayan Sequence and calculated inverted gradients beneath the Vaikrita thrust to be ~40 °C/km. An inverted thermal field gradient has also been documented beneath a klippe that lies ~25 km south of the Vaikrita thrust. The Askot klippe sits atop a region where the background peak temperature of Lesser Himalayan Sequence rocks is ~370 °C. A suite of seven samples beneath the klippe reveals an inverted thermal field gradient of ~20 °C/km and a peak in footwall temperature of 530 °C at the base of the klippe. The spatial association of peaks in RSCM temperatures and proximity to the hanging wall of the Main Central thrust lead us to interpret the mechanism for thermal metamorphism in the Lesser Himalayan Sequence to be conduction of heat from the Main Central thrust fault and/or hanging wall to the footwall. In addition to the spatial association between the Main Central thrust and the temperature maxima in the Lesser Himalayan Sequence, the Tons thrust shows a localized thermal signature associated with it, which lends support to the models requiring a large offset along the structure. The presence of kyanite in quartzites

adjacent to graphitic rocks that record peak metamorphic temperatures of ~550 °C constrains pressure to be ≥5 kbar.

The $^{40}Ar/^{39}Ar$ white mica ages indicate that the exposed rocks closed with respect to Ar loss at various intervals in the late Tertiary. The proximal footwall of the Munsiari thrust experienced closure at ca. 8.5 Ma. South of Munsiari thrust, in the proximal footwalls of the Chaukori and Askot klippen, muscovites ages are ca. 11.5 Ma, or ~3 Ma older than samples to the north. The age differences in samples from northern and southern exposures are interpreted to document cooling related to thermal relaxation following passage of the Main Central thrust hanging wall atop the Lesser Himalayan Sequence. A single 4.3 Ma cooling age obtained from a Berinag quartzite at the type locality of the Munsiari thrust is consistent with models advocating out-of-sequence faulting along the Munsiari thrust. Despite the significance of the Main Boundary, Tons, and Berinag thrusts in the construction of the Lesser Himalayan Sequence, these structures do not appear to have influenced closure of the $^{40}Ar/^{39}Ar$ white mica chronometer.

Results of thermo-kinematic modeling show that the thermal history data obtained from the Kumaun and Garwhal Lesser Himalayan Sequence can be well fit by a two-stage evolutionary scenario. Good fits between the models and data were achieved assuming the following thermal evolution for the Lesser Himalayan Sequence: an early Miocene phase of overthrusting of a hot hanging wall over a downgoing footwall, followed by the initiation of a duplex within the Lesser Himalayan Sequence.

REFERENCES CITED

Ahmad, T., Harris, N., Bickle, M., Chapman, H., Bunbury, J., and Prince, C.I., 2000, Isotopic constraints on the structural relationships between the Lesser Himalayan Series and the High Himalayan Crystalline Series, Garwhal Himalaya: Geological Society of America Bulletin, v. 112, no. 3, p. 467–477, doi: 10.1130/0016-7606(2000)112<0467:ICOTSR>2.3.CO;2.

Arita, K., Dallmeyer, R.D., and Takasu, A., 1997, Tectonothermal evolution of the Lesser Himalaya, Nepal: Constraints from Ar-40/Ar-39 ages from the Kathmandu nappe: The Island Arc, v. 6, p. 372–385, doi: 10.1111/j.1440-1738.1997.tb00047.x.

Armijo, R., Tapponnier, P., Mercier, J.L., and Han, T.L., 1986, Quaternary extension in southern Tibet—Field observations and tectonic implications: Journal of Geophysical Research–Solid Earth and Planets, v. 91, p. 13,803–13,872.

Auden, J.B., 1935, Traverses in the Himalaya: Records of the Geological Society of India, v. 69, p. 123–167.

Avouac, J.P., 2003, Mountain building, erosion and the seismic cycle in the Nepal Himalaya, *in* Dmowska, R., ed., Advances in Geophysics: Amsterdam, Elsevier, p. 1–79.

Avouac, J.P., 2008, Mountain building: From earthquakes to geological deformation, *in* Schubert, G., ed., Dynamic Processes in Extensional and Compressional Settings: Treatise on Geophysics: Amsterdam, Elsevier, p. 377–439.

Beaumont, C., Jamieson, R.A., Nguyen, M.H., and Lee, B., 2001, Himalayan tectonics explained by extrusion of a low-viscosity crustal channel coupled to focused surface denudation: Nature, v. 414, p. 738–742.

Beaumont, C., Jamieson, R.A., Nguyen, M.H., and Medvedev, S., 2004, Crustal channel flows: 1. Numerical models with applications to the tectonics of the Himalayan-Tibetan orogen: Journal of Geophysical Research, v. 109, B06406, doi: 10.1029/2003JB002809.

Bettinelli, P., Avouac, J.P., Flouzat, M., Jouanne, F., Bollinger, L., Willis, P., and Chitraker, G.R., 2006, Plate motion of India and interseismic strain in the Nepal Himalaya from GPS and DORIS measurements: Journal of Geodesy, doi: 10.1007/s00190-006-0030-3,2006.

Beyssac, O., Goffe, B., Chopin, C., and Rouzaud, J.N., 2002, Raman spectra of carbonaceous material in metasediments: A new geothermometer: Journal of Metamorphic Geology, v. 20, p. 859–871, doi: 10.1046/j.1525-1314.2002.00408.x.

Beyssac, O., Goffé, B., Petitet, J.P., Froigneux, E., Moreau, M., and Rouzaud, J.N., 2003, On the characterization of disordered and heterogeneous carbonaceous materials by Raman spectroscopy: Spectrochimica Acta, Part A–Molecular and Biomolecular Spectroscopy, v. 59, no. 10, p. 2267–2276.

Beyssac, O., Bollinger, L., Avouac, J.P., and Goffe, B., 2004, Thermal metamorphism in the Lesser Himalaya of Nepal determined from Raman spectroscopy of carbonaceous material: Earth and Planetary Science Letters, v. 225, p. 233–241, doi: 10.1016/j.epsl.2004.05.023.

Bilham, R., Larson, K., and Freymueller J., 1997, GPS measurements of present-day convergence across the Nepal Himalaya: Nature, v. 386, p. 61–64, doi: 10.1038/386061a0.

Bollinger, L., et al., 2004, Thermal structure and exhumation history of the Lesser Himalaya in central Nepal: Tectonics, v. 23, TC5015, doi: 10.1029/2003TC001564,2004.

Bollinger, L., et al., 2006, Mountain building in the Nepal Himalaya: Thermal and kinematic model: Earth and Planetary Science Letters, v. 244, p. 58–71, doi: 10.1016/j.epsl.2006.01.045.

Braun, J., 2003, Pecube: A new finite-element code to solve the 3D heat transport equation including the effects of a time-varying, finite amplitude surface topography: Computers & Geosciences, v. 29, p. 787–794, doi: 10.1016/S0098-3004(03)00052-9.

Burg, J.P., and Gerya, T., 2005, Viscous heating and thermal doming in orogenic metamorphism: Numerical modelling and geological implications: Journal of Metamorphic Geology, v. 23, p. 75–95, doi: 10.1111/j.1525-1314.2005.00563.x.

Catlos, E.J., Harrison, T.M., Kohn, M.J., Grove, M., Ryerson, F.J., Manning, C.E., and Upreti, B.N., 2001, Geochronologic and thermobarometric constraints on the evolution of the Main Central thrust, central Nepal Himalaya: Journal of Geophysical Research, Ser. B, Solid Earth and Planets, v. 106, p. 16,177–16,204.

Catlos, E.J., Dubey, C.S., Marston, R.A., and Harrison, T.M., 2007, Deformation within the Main Central Thrust Shear Zone, Bhagirathi River (NW India): Implications for Himalayan Tectonics, *in* Cloos, M., Carlson, W.D., Gilbert, M.C., Liou, J.G., and Sorensen, S.S., eds., Convergent Margin Terranes and Associated Regions: A tribute to W. G. Ernst: Geological of America Special Paper 419, p. 135-151.

Cattin, R., and Avouac, J.-P., 2000, Modeling of mountain building and the seismic cycle in the Himalaya of Nepal: Journal of Geophysical Research, v. 105, p. 13,389–13,407, doi: 10.1029/2000JB900032.

Célérier, J., 2007, The structural and thermal evolution of the Kumaun and Garwhal Lesser Himalaya, India [Ph.D. thesis]: The Australian National University.

Célérier, J., Harrison, T.M., Yin, A., and Webb, A.A.G., 2009, The Kumaun and Garwhal Lesser Himalaya, India. Part 1: Structure and stratigraphy: Geological Society of America Bulletin (in press).

Copeland, P., Harrison, T.M., Hodges K.V., Maruejol, P., Lefort P., and Pêcher, A., 1991, An early Pliocene thermal disturbance of the Main Central thrust, central Nepal—Implications for Himalayan tectonics: Journal of Geophysical Research, Ser. B, Solid Earth and Planets, v. 96, p. 8475–8500, doi: 10.1029/91JB00178.

DeCelles, P.G., Robinson, D.M., Quade J., Ojha, T.P., Garzione, C.N., Copeland, P., and Upreti, B.N., 2001, Stratigraphy, structure, and tectonic evolution of the Himalayan fold-thrust belt in western Nepal: Tectonics, v. 20, p. 487–509, doi: 10.1029/2000TC001226.

Dickinson, W., 1971, Plate tectonics in geologic history: Science, v. 174, p. 107–113, doi: 10.1126/science.174.4005.107.

Dodson, M.H., 1986, Closure profiles in cooling systems, *in* Material Science Forum: Aedermannsdorf, Switzerland, Trans Tech Publications, p. 145–153.

Dunlap, W.J., 1997, Neocrystallization or cooling? Ar-40/Ar-39 ages of white micas from low-grade mylonites: Chemical Geology, v. 143, p. 181–203, doi: 10.1016/S0009-2541(97)00113-7.

Dunlap, W.J., Hirth G., and Teyssier, C., 1997, Thermomechanical evolution of a ductile duplex: Tectonics, v. 16, p. 983–1000, doi: 10.1029/97TC00614.

Edwards, R.M., 1995, $^{40}Ar/^{39}Ar$ geochronology of the Main Central thrust (MCT) region: Evidence for late Miocene to Pliocene disturbances along the MCT, Marsyangdi River valley, west-central Nepal Himalaya: Journal of Nepal Geological Society, v. 10, p. 41–46.

Engelder, T., 1993, Stress regimes in the Lithosphere: Princeton, Princeton University Press, 451 p.

England, P., and Molnar, P., 1993, The interpretation of inverted metamorphic isograds using simple physical calculations: Tectonics, v. 12, no. 1, p. 145–157, doi: 10.1029/92TC00850.

England, P.C., and Thompson, A., 1984, Pressure-temperature-time paths of regional metamorphism: 1. Heat transfer during the evolution of regions of thickened continental crust: Journal of Petrology, v. 25, p. 894–928.

England, P.C., Le Fort, P., Molnar, P., and Pêcher, A., 1992, Heat sources for Tertiary metamorphism and anatexis in the Annapurna-Manaslu region (central Nepal): Journal of Geophysical Research, v. 97, p. 2107–2128, doi: 10.1029/91JB02272.

Ernst, W.G., 1971, Do mineral parageneses reflect unusually high pressure conditions of Franciscan metamorphism?: American Journal of Science, v. 270, p. 81–108.

Ferry, J.M., and Spear, F.S., 1978, Experimental calibration of partitioning of Fe and Mg between biotite and garnet: Contributions to Mineralogy and Petrology, v. 66, p. 113–117, doi: 10.1007/BF00372150.

Graham, C.M., and England, P.C., 1976, Thermal regimes and regional metamorphism in vicinity of overthrust faults—An example of shear heating and inverted metamorphic zonation from Southern California: Earth and Planetary Science Letters, v. 31, no. 1, p. 142–152, doi: 10.1016/0012-821X(76)90105-9.

Hansen, F., and Carter, N., 1982, Creep of selected crustal rocks at 1000 MPa: Eos (Transactions, American Geophysical Union), v. 63, p. 437.

Harrison, T.M., Ryerson F.J, Le F.P., Yin, A., Lovera, O.M., and Catlos, E.J., 1997, A late Miocene–Pliocene origin for the central Himalayan inverted metamorphism: Earth and Planetary Science Letters, v. 146, p. E1–E7, doi: 10.1016/S0012-821X(96)00215-4.

Harrison, T.M., Grove, M., Lovera, O.M., and Catlos E.J., 1998, A model for the origin of Himalayan anatexis and inverted metamorphism: Journal of Geophysical Research, Ser. B, Solid Earth and Planets, v. 103, p. 27,017–27,032, doi: 10.1029/98JB02468.

Harrison, T.M., Grove, M., D.A.J., Catlos, E.J., and Lovera, O.M., 1999a, Models for the thermal and tectonic evolution of southern Tibet and the Himalaya, *in* AGU 1999 Fall meeting, v. 80, no. 46, suppl.: Washington, D.C., American Geophysical Union, p. 989–990.

Harrison, T.M., Grove, M., Lovera, O.M., and Catlos, E.J., DAJ, 1999b, The origin of Himalayan anatexis and inverted metamorphism: Models and constraints, *in* Geology of the Nepal Himalaya; Recent Advances, Volume 17; 5–6: Oxford, Pergamon, p. 755–772.

Harrison, T.M., Célérier, J., Aikman, A.B., Hermann, J., and Heizler, M.T., 2009, Diffusion of ^{40}Ar in muscovite: Geochimica et Cosmochimica Acta, v. 73, p. 1039–1051, doi: 10.1016/j.gca.2008.09.038.

Hashimoto, S., Ohta, Y., and Akiba, C., 1973, Geology of the Nepal Himalayas: Tokyo, Saikon, 286 p.

Hauck, M.L., Nelson, K.D., Brown, L.D., Zhao, W.J., and Ross, A.R., 1998, Crustal structure of the Himalayan orogen at ~90° east longitude from Project INDEPTH deep reflection profiles: Tectonics, v. 17, p. 481–500, doi: 10.1029/98TC01314.

Herman, F., Braun, J., and Dunlap, W.J., 2007, Tectonomorphic scenarios in the Southern Alps of New Zealand: Journal of Geophysical Research, v. 112, p. B04201, doi: 10.1029/2004JB003472.

Hirth, G., and Tullis, J., 1992, Dislocation creep regimes in quartz aggregates: Journal of Structural Geology, v. 14, p. 145–159, doi: 10.1016/0191-8141(92)90053-Y.

Holdaway, M.J., 1971, Stability of andalusite and aluminum silicate phase diagram: American Journal of Science, v. 271, p. 97.

Hubbard, M.S., and Harrison, T.M., 1989, $^{40}Ar/^{39}Ar$ age constraints on deformation and metamorphism in the Main Central thrust zone and Tibetan slab, eastern Nepal Himalaya: Tectonics, v. 8, p. 865–880, doi: 10.1029/TC008i004p00865.

Jamieson, R.A., Beaumont, C., Medvedev, S., and Nguyen, M.H., 2004, Crustal channel flows: 2. Numerical models with implications for metamorphism in the Himalayan-Tibetan orogen: Journal of Geophysical Research, v. 109, B06406, doi: 10.1029/2003JB002811.

Kerrick, D.M., 1990, The Al_2SiO_5 polymorphs: Reviews in Mineralogy, v. 22, 406 p.

Kohn, M.J., Catlos, E.J., Ryerson, F.J., and Harrison, T.M., 2001, Pressure-temperature-time path discontinuity in the Main Central thrust zone, central Nepal: Geology, v. 29, p. 571–574, doi: 10.1130/0091-7613(2001)029<0571: PTTPDI>2.0.CO;2.

Kong, X., and Bird, P., 1996, Neotectonics of Asia: Thin-shell, finite-element models with faults, *in* Yin, A., and Harrison, T.M., eds., Tectonics of Asia: New York, Cambridge University Press, p. 18–35.

Lavé, J., and Avouac, J.P., 2000, Active folding of fluvial terraces across the Siwaliks Hills, Himalayas of central Nepal: Journal of Geophysical Research, Ser. B, Solid Earth and Planets, v. 105, p. 5735–5770, doi: 10.1029/1999JB900292.

Lavé, J., and Avouac, J.P., 2001, Fluvial incision and tectonic uplift across the Himalayas of central Nepal: Journal of Geophysical Research, Ser. B, Solid Earth and Planets, v. 106, p. 26,561–26,591, doi: 10.1029/2001JB000359.

LeFort, P., 1975, Himalayas: The collided range. Present knowledge of the continental arc: American Journal of Science, v. 275-A, p. 1–44.

Le Fort, P., 1996, Evolution of the Himalaya, *in* Yin, A., and Harrison, T.M., eds., The Tectonic Evolution of Asia: New York, Cambridge University Press, p. 95–106.

McDougall, I., and Harrison, T.M., 1999, Geochronology and Thermochronology by the $^{40}Ar/^{39}Ar$ Method

(2nd edition): Oxford, Oxford University Press, v. 20, p. 26–40.

Medicott, H.B., 1864, On the Geologic Structure and Relations of the Southern Portion of the Himalayan Range between the Rivers Ganges and Ravee: Geological Survey of India Memoir 3, 206 p.

Middlemiss, C.S., 1887, Physical geology of the West British Garwhal; with notes on a route traverse through Jaunsar Bawar and Tiri-Garwhal: Records of the Geological Survey of India, v. 20, p. 26–40.

Molnar, P., and England, P., 1990, Temperatures, heat-flux, and frictional stress near major thrust faults: Journal of Geophysical Research, Ser. B, Solid Earth and Planets, v. 95, no. B4, p. 4833–4856, doi: 10.1029/JB095iB04p04833.

Oldham, R.D., 1883, The geology of Jaunsar and the Lower Himalayas: Records of the Geological Survey of India, v. 16, p. 193–198.

Paudel, L.P., and Arita, K., 2000, Tectonic and polymetamorphic history of the Lesser Himalaya in central Nepal: Journal of Asian Earth Sciences, v. 18, p. 561–584, doi: 10.1016/S1367-9120(99)00069-3.

Pêcher, A., 1989, The metamorphism in the central Himalaya: Journal of Metamorphic Geology, v. 7, no. 1, p. 31–41, doi: 10.1111/j.1525-1314.1989.tb00573.x.

Richards, A., Argles T., Harris N., Parrish R., Ahmad, T., Darbyshire, F., and Draganits, E., 2005, Himalayan architecture constrained by isotopic tracers from clastic sediments: Earth and Planetary Science Letters, v. 236, p. 773–796, doi: 10.1016/j.epsl.2005.05.034.

Robinson, D.M., DeCelles P.G., Garzione, C.N., Pearson, O.N., Harrison T.M., and Catlos, E.J., 2003, Kinematic model for the Main Central thrust in Nepal: Geology, v. 31, p. 359–362, doi: 10.1130/0091-7613(2003)031<0359:KMFTMC>2.0.CO;2.

Robinson, D.M., DeCelles, P.G., and Copeland P., 2006, Tectonic evolution of the Himalayan thrust belt in western Nepal: Implications for channel flow models: Geological Society of America Bulletin, v. 118, p. 865–885, doi: 10.1130/B25911.1.

Ruppel, C., and Hodges, K.V., 1994, Pressure-temperature-time paths from 2-dimensional thermal models—Prograde, retrograde and inverted metamorphism: Tectonics, v. 13, p. 17–44, doi: 10.1029/93TC01824.

Rutter, E.H., 1997, The influence of deformation on the extraction of crustal melts: A consideration of melt assisted granular flow, *in* Holmes, M.B., ed., Deformation-Enhanced Fluid Transport in Earth's Crust and Mantle: London, Chapman & Hall, p. 82–110.

Schelling, D., and Arita, K., 1991, Thrust tectonics, crustal shortening and the structure of the far-eastern Nepal Himalaya: Tectonics, v. 10, p. 851–862, doi: 10.1029/91TC01011.

Schulte-Pelkum, V., Monsalve, G., Sheehan, A., Pandey, M.R., Sapkota, S., Bilham, R., and Wu, F., 2005, Imaging the Indian subcontinent beneath the Himalaya: Nature, v. 435, p. 1222–1225, doi: 10.1038/nature03678.

Shi, Y.L., and Wang, C.Y., 1987, Two-dimensional modeling of the *P-T-t* paths of regional metamorphism in simple overthrust terrains: Geology, v. 15, p. 1048–1051, doi: 10.1130/0091-7613(1987)15<1048:TMOTPP>2.0.CO;2.

Suppe, J., 1983, Geometry and kinematics of fault-bend folding: American Journal of Science, v. 283, p. 684–721.

Valdiya, K.S., 1980, Geology of the Kumaun Lesser Himalaya: Dehra Dun, India, Wadia Institute of Himalayan Geology, 291 p.

Vannay, J.-C., and Grasemann, B., 1998, Inverted metamorphism in the High Himalaya of Himachal Pradesh (NW India): Phase equilibria versus thermobarometry: Schweizerische Mineralogische und Petrographische Mitteilungen, v. 78, p. 107–132.

Vannay, J.-C., Grasemann, B., Rahn, M., Frank, W., Carter, A., Baudraz, V., and Cosca, M., 2004, Miocene to Holocene exhumation of metamorphic crustal wedges in the NW Himalaya: Evidence for tectonic extrusion coupled to fluvial erosion: Tectonics, v. 23, TC1014, doi: 10.1029/2002TC001429,2004.

Zhao, W., Nelson, K.D., Che, J., Guo, J., Lu, D., Wu, C., Liu, X., Brown, L.D., Hauck, M.L., Kuo, J.T., Klemperer, S., and Makovsky, Y., 1993, Deep seismic reflection evidence for continental underthrusting beneath southern Tibet: Nature, v. 366, p. 557–559, doi: 10.1038/366557a0.